DESIGN FEATURES OF TOKAMAK POWER REACTORS WITH RF-DRIVEN STEADY STATE CURRENT

S. Y. Yuen, J. H. Schultz,
D. Kaplan and D. Cohn

November, 1979
M.I.T. Plasma Fusion Center Report RR-79-22

DESIGN FEATURES OF TOKAMAK POWER REACTORS WITH RF-DRIVEN STEADY STATE CURRENT*

S. Y. Yuen, J. H. Schultz,
D. Kaplan and D. Cohn

M.I.T. Plasma Fusion Center†

and

Francis Bitter National Magnet Laboratory††

M.I.T. Plasma Fusion Center
Report RR-79-22

* Work supported by U.S. D.O.E. Contract
† Supported by D.O.E.
†† Supported by N.S.F.

TABLE OF CONTENTS

TABLE OF CONTENTS
(continued)

1. EXECUTIVE SUMMARY

This report investigates the feasibility of a steady state tokamak power reactor driven by lower hybrid waves. Our results indicate that such a reactor may be possible, and the characteristics of a reference steady state reactor are presented. Special emphasis is made to identify the constraints and potential problems involved in the steady state current-drive scheme that need further study. The physics and engineering results are summarized in sections 1.2 and 1.3, respectively. Section 1.4 presents the main conclusions and Section 1.5 discusses some problems requiring further studies.

1.1 INTRODUCTION

The use of radio frequency (rf) waves near the lower hybrid frequency to drive steady state electron current in tokamaks has been proposed recently.[1,2] In the proposed scheme, a continuous current is generated by electron Landau damping of rf waves traveling in only one direction parallel to the magnetic field. The wave carries net parallel momentum, which, when absorbed by resonant electrons, drives the toroidal current necessary for plasma confinement. With this scheme, steady state tokamak operation becomes possible.

The engineering advantages of the steady-state, rf-driven reactor include an improved reactor duty cycle, elimination of a thermal storage system, lower recirculating losses

in the poloidal field system, lower cost of the poloidal field system, lower cost and high maintainability of an rf system over a neutral beam heated system, and lower crack growth in the first wall and blanket due to cycling. The disadvantages include recirculating losses in the rf system and more stringent impurity control requirements.

The conceptual design of an rf-driven, steady state tokamak experiment has been carried out at General Atomics.[3] There has also been a study on the design constraints of steady state tokamak power reactors confined by rf-driven currents.[4] The present study differs from Ref. 4 in several major ways:

1) The present reactor designs are based on centrally peaked current profiles, instead of surface currents considered in Ref. 4. The reason for using centrally peaked current profile is to minimize extrapolation from experimentally established MHD stability in tokamak devices. The reference design in this report duplicates the plasma of the High Field Compact Tokamak Reactor (HFCTR).[5]

2) The hot ion mode operation,[6] i.e., the decoupling of electron and ion temperatures at ignition and high ion temperature, is identified as a means to enhance the ratio of fusion power output to dissipated wave power.

3) Accessibility and propagation of the lower hybrid wave in plasma is taken in account in detail. Effects of possible nonlinearities are examined.

4) High efficiency microwave components are identified and a microwave circuit designed.

5) Direct recovery of the reflected rf wave is introduced to relieve the stringent requirement on wave-plasma coupling efficiency while maintaining the same plant efficiency.

6) A comparison of the overall plant efficiency and cost of the original HFCTR design and the present rf-current-drive system has been made.

1.2 WAVE-PLASMA COUPLING AND CURRENT GENERATION

Special attention is paid in this study to the figure of merit Q, defined as the ratio of fusion power output to the dissipated wave power for current generation. With due consideration of constraints imposed by wave-plasma coupling processes, Q is varied over a wide range in parameter space. The maximun Q occurs for average electron temperature $\overline{T}_e \simeq 16$ keV. At such temperature, the electron and ion temperatures decouple and $\overline{T}_e < \overline{T}_i$. Besides enhancing Q, this "hot ion mode" operation also leads to longer thermal runaway time and, hence, reduces poloidal field coil requirements.

It is also found that Q increases with magnetic field as well as plasma density. Thus steady state current generation by lower hybrid wave is especially suitable for high field, high power density tokamak power reactor designs. The parameters for a reference reactor with moderate size, high field, high power density, and a Q of 40 are given in Table 1.

The physics problems involved in the rf-current drive scheme can be divided into two parts: the current generation process itself and how the wave gets to where the current is to be generated. Experimental evidence for the existence of the former is meager at present, but several experiments are either underway or are being planned. They will be summarized in Section 2.2. Considerable data on wave propagation are available from recent lower hybrid heating experiments. Some of the observed phenomena may be unfavorable for the current generating purpose. The experimental data will be reviewed and their implications for steady state current-drive discussed in Sections 3.1 and 3.3.

1.3 REACTOR ENGINEERING

Two engineering aspects for the steady-state current-driven tokamak reactor have been studied. Firstly, a high-efficiency microwave delivery system has been identified. Secondly, a rough cost estimate has been made comparing the reference steady-state reactor specified in Table 1 with the

original HFCTR design. It should be pointed out here that the differences between the two reactor designs lie not only in steady-state operation, but also in hot ion mode operation and the use of a long-pulsed, lower hybrid microwave power delivery system.

A microwave circuit designed primarily for high-efficiency, rather than low initial cost, has been identified. Microwave power reflected from the plasma due to imperfect wave-plasma coupling can be retrieved through the direct energy recovery channel. A 50% efficient microwave delivery system could be built with previously developed benchmark components. With a device development program, an overall efficiency of 75% can be projected. Such high microwave efficiency facilitates economical operation of a moderate-Q plasma in a steady-state tokamak reactor.

Steady-state operation retards crack growth rate but does not prevent swelling or embrittlement of the first wall, as discussed in Section 6.2.B. Thus there may be no first-order gain in stainless-steel first wall life operating at 450° C if only normal operation conditions are considered. However, both pulsed and steady-state operations are susceptible to first wall degradation and destruction by plasma disruption, and disruptions may be less lilely in the steady-state case.

The elimination of thermal energy storage by steady-state operation is not found to be a major cost consideration, as

discussed in Section 6.2.C. Impurity and alpha-particle control problems in a steady-state reactor are not substantially different from that for pulsed reactors with burn periods long compared with alpha build-up times, typically 100 seconds.

With rf-assisted start-up and current-drive, moderate reductions in equilibrium field coil power and strong reduction in ohmic heating coil power appear to be possible. Parasitic losses in generators, transformers, and rectifiers associated with the high-pulsed poloidal field coil power can be reduced by the use of rf-assisted start-up alone. The equilibrium coil power required for plasma thermal stability control during burn is reduced for hot ion mode operation because of its long thermal runaway time. However, hot ion mode operation also makes reactor ripple requirements more stringent and, hence, complicates divertor design. An assessment of the competing effects, in comparison with the pulsed HFCTR design, is presented in Section 6.2.E.

1.4 SUMMARY AND CONCLUSIONS

The feasibility, the plasma and engineering characteristics, and economic implications of steady-state tokamak power reactors with rf-driven current have been studied. A wide reactor parameter space is surveyed, and a reference steady-state power reactor compatible with the High Field Compact Tokamak Reactor (HFCTR) [5] is considered in specific. The following results emerge from this study:

1) Steady state current generation by lower hybrid wave is especially suitable for high field, high density tokamak power reactor designs, as Q increases both with magnetic field and plasma density (Q = fusion power / rf power dissipated by current generation).

2) For a moderate size (R = 6m), high field (B_0=7.5T), high power density (P_F = 9.1 MW/m^3) reactor of the HFCTR configuration, values of Q as high as 40 may be obtained for a centrally peaked parabolic current profile. Even higher Q can be attained if the current is more concentrated near the plasma edge.

3) The recirculating power required for such high Q steady state reactors may not be higher than that for a pulsed, ignited reactor.

4) For high Q operations, the steady state current driven reactor may potentially reduce the cost of electricity by up to a factor of two when compared to a pulsed tokamak reactor.

5) The hot ion mode ($T_e < T_i$) operation is advantageous for the steady state reactor in several ways: Q is increased by about 30%; the optimum operating electron temperature is lowered; and the thermal runaway rate is greatly reduced.

6) The availability of efficient, high power, continuous-wave microwave delivery system makes steady state current driven by lower hybrid wave more attractive than current-

drive schemes using higher frequency waves.

7) The high magnetic field requirements may be relaxed by increasing the major radius of the reactor; allowing the current to concentrate near the plasma edge; operating at Lower Q.

1.5 PROBLEMS REQUIRING FURTHER STUDY

This report presents a first-cut study of the feasibility of a steady state power reactor utilizing rf-driven currents. Due to the lack of experimental data and the full theoretical understanding of the physics involved, the study is based on several major assumptions and approximations; these assumptions and approximations are discussed in sections 5.3 and 6.2.E. A number of further outstanding problems remain.

(1) High intensity and high temperature effects: the present study is based on the quasi-linear theory. High wave intensity and high plasma temperature may introduce nonlinear and relativistic effects which will modify the value of Q.

(2) Startup: the present study considers only the case where the reactor is already in steady state operation. The startup of a steady state reactor has not been examined. An attractive

option is to start with a very low temperature discharge and use rf wave for heating as well as current drive. Such a scenario may eliminate most of the ohmic transformer but will require a rf system with variable frequency and spectrum. Without extensive transport calculations and technological advances in microwave systems, such an option remains speculative.

(3) Nonlinear effects: nonlinear effects observed in recent tokamak heating experiments will be deleterious to the current driving scheme (see section 3.3). These effects should be thoroughly understood and prevented in the steady state reactor.

(4) Control of plasma edge characteristics: turbulence at the plasma edge may prevent wave penetration or scatter the wave. It is desirable if the plasma edge characteristics can be controlled in a reactor. Interaction of the mainly toroidally-directed travelling wave with a divertor-created scrape-off layer may suppress current generation at the plasma edge.

(5) Current profile: the present study is based on centrally peaked parabolic profiles. Other current profiles, for example the skin current configuration of Ref. 4, can have higher Q or require lower magnetic field, thus making the steady state reactor version even more attractive. The equilibrium and stability of these current profile configurations need to be studied taking into account classical MHD as well as various microinstabilities.

(6) Waveguide design: the characteristics of waveguide arrays consisting of fifteen or more elements need further study. Effects of possible coupling between adjacent waveguide arrays should also be investigated.

(7) The effect of impurity concentration on the efficiency of steady state current generation should be studied.

It is clear that the above questions must be resolved experimentally, as well as theoretically, before the feasibility of a rf-driven steady state tokamak power reactor can be fully assessed.

2. CURRENT GENERATION BY RF WAVE

2.1 QUASI-LINEAR THEORY FOR CURRENT GENERATION

Consider an rf wave with energy $\mathcal{E}$, parallel phase velocity v_z, and frequency ω traveling in a plasma with electron temperature T_e and density n_e. The wave distorts the electron distribution and produces a plateau in the region of resonant particles. Binary collisions of the resonant particles with other plasma particles tends to restore thermal equilibrium, thus establishing stationary wave absorption.

Since the wave travels in only one direction, the asymmetric electron distribution thus created will result in a net current in the direction of the wave's phase velocity.

After averaging over velocities perpendicular to the magnetic field, the one dimensional quasi-linear equation for an electron distribution function f in the presence of rf field is given by [7]:

$$\frac{\partial f}{\partial \tau} = \frac{\partial}{\partial u}\left[\left(D + \frac{1}{2u^3}\right)\frac{\partial f}{\partial u} + \frac{f}{u^2}\right] \qquad (1)$$

where

$$u = v_z/v_{Te}$$

$$v_{Te} = (2T_e/m_e)^{1/2}$$

$$\tau = \nu u^3 t$$

$$\nu = 4\pi(Z_i + 2)n_e e^4 \ell n\Lambda/m_e^2 v_z^3$$

$$D = D_{QL}/\nu u^3 v_{Te}^2 \simeq [8\pi/(Z_i + 2)](1/n_e e^4 u \ell n\Lambda)[\mathcal{E}_{kz}/\partial(\varepsilon_R\omega)/\partial\omega].$$

D_{QL} is the quasi-linear diffusion coefficient, Z_i the charge of the ion species, and ε_R the real part of the dielectric function of the lower hybrid wave. In the steady state, the electron flux in velocity space vanishes, and the solution of Eq. (1) is given by:

$$f(u) = \begin{cases} C\, e^{-u^2} & u < u_1 \\ C\, e^{-u_1^2}\left[\dfrac{2D_o u_1^2 + 1}{2D_o u^2 + 1}\right]^{1/2D_o} & u_1 \le u \le u_2 \\ C\, e^{u_2^2 - u_1^2}\left[\dfrac{2D_o u_1^2 + 1}{2D_o u_2^2 + 1}\right]^{1/2D_o} e^{-u^2} & u_2 < u \end{cases} \quad (2)$$

where $D_o = Du$ and the constant C is determined by $\int f(u)\, du = 1$. In Eq. (2), the rf wave spectrum is assumed to be

$$\mathcal{E}_{kz} = \mathcal{E}/\Delta k_z \qquad u_1 \le u \le u_2 \qquad (3)$$

and zero elsewhere, $\Delta k_z = k_{z1} - k_{z2} = (\omega/u_1 - \omega/u_2)/v_{Te}$.

With large rf power flux, $D_o u^2 >> 1$, Eq. (2) reduces to

$$f(u) = \begin{cases} C \exp(-u^2) & u < u_1 \\ C \exp(-u_1^2) & u_1 \leq u \leq u_2 \\ C \exp(-u_1^2 + u_2^2 - u^2) & u > u_2 \end{cases} \quad (4)$$

with $C = [\sqrt{\pi} + (u_2 - u_1) \exp(-u_1^2)]^{-1}$. The electron distribution Eq. (4) is shown schematically in Fig. 1. It can be seen that the electron distribution function at $u > u_2$ greatly exceeds the original Maxwellian distribution. Thus current is carried not only by resonant electrons with $u_1 \leq u \leq u_2$, but also by the tail electrons with $u > u_2$. Figure 2 shows the fraction of total current carried by resonant electrons under the plateau. In reactor type plasmas, $u_1 \lesssim 2$, $u_2 \lesssim 2.5$, half or more of the current generated by rf wave will be carried by the fast tail electrons.

The current density generated can at once be obtained from Eq. (2) by integrating over velocity space

$$J = \frac{1}{2} n_e e v_{Te} f_m(u_1)\, C \left\{ \frac{(2D_o u_1^2 + 1)^{1/2D_o}}{(2D_o - 1)} \left[(2D_o u_2^2 + 1)^{1-1/2D_o} - (2D_o u_1^2 + 1)^{1-1/2D_o} \right] + \left(\frac{2D_o u_1^2 + 1}{2D_o u_2^2 + 1} \right)^{1/2D_o} - 1 \right\} \quad (5)$$

which, when $D_o u^2 >> 1$, reduces to

$$J = \frac{1}{2} n_e e v_{Te} f_m(u_1)[1 + f_m(u_1)(u_2 - u_1)]^{-1}(u_2^2 - u_1^2) \tag{6}$$

$$= 8.5 \times 10^7 n_{20} T_e^{1/2}[1 + f_m(u_1)(u_2 - u_1)]^{-1}\exp(-u_1^2)$$
$$(u_2^2 - u_1^2) \qquad A/m^2 \tag{6a}$$

where $f_m(u) = (1/\sqrt{\pi})\ \exp(-u^2)$, $n_{20} = n_e/10^{20}\ m^{-3}$, and temperatures are given in KeV.

The variation of rf power flux as it penetrates radially into the plasma can be derived from quasi-linear results [7]

$$\frac{1}{r}\frac{\partial}{\partial r}(r v_{g_\perp} \mathcal{E}_{kz}) = -2\gamma_{kz}\mathcal{E}_{kz} \tag{7}$$

$$\gamma_{kz} = \frac{\gamma_{okz}}{1 + 2Du^3} = \sqrt{\frac{\pi}{8}}\ \frac{\omega^2}{(1 + \omega_{pe}^2/\Omega_e^2)\omega_{pe}(k_z\lambda_D)^3}\ \frac{1}{1 + 2Du^3}\ e^{-u^2} \tag{8}$$

Here, γ_{kz} is the quasi-linear corrected damping rate, $v_{g_\perp} = \partial\omega/\partial k_\perp$ is the perpendicular group velocity, ω_{pe}, Ω_e the electron plasma and cyclotron frequencies, and λ_D the Debye wavelength. All of these quantities are a function of r through density, temperature and magnetic field profiles. The power dissipation density of an rf wave with spectral width Δk_z is given by:

$$P_D = \int_{k_{z2}}^{k_{z1}} 2\gamma_{kz}\mathcal{E}_{kz}\, dk_z \tag{9}$$

When $Du^3 >> 1$, Eq. (9) can be approximated as:

$$P_D = \frac{1}{2}\nu u_1^3 \, v_{Te}^2 n_e m_e (\partial \varepsilon_R \omega/\partial\omega) f_m(u_1) \ell n(u_2/u_1) K \qquad (10)$$

$$= 9 \times 10^9 \, n_{20}^2 T_e^{-1/2} \exp(-u_1^2) \ell n(u_2/u_1) K. \qquad W/m^3 \quad (10a)$$

In reality, the lower hybrid wave propagates in a well-defined resonance cone. However, since we are only interested in power dissipation and current generation, toroidal and azimuthal variations will be averaged out by electrons streaming in and out of the resonance cone. Thus, Eq. (7) will form a model for the radial propagation of the rf wave. The total power dissipated by the rf wave is given by

$$P_{rf} = 4\pi^2 R \int^{\bar{a}} P_D r dr$$

where $\overline{a^2} = a^2(2S^2-1)^{1/2}$, and the shape factor S is defined by S = plasma circumference/$2\pi a$.

Equation (10a) is obtained with $Z_i = 1$. Examining Eq. (6) and (10) show that while the current generated is independent of Z_i. The power dissipated scales as $(2 + Z_i)/3$. Higher Z_i increases the collisionality of the plasma, hence more rf power is required to maintain the current carrying plateau in the electron distribution function. Except for the factor K, Eq. (9) is the same result derived in Refs. [1,2] by integrating

the collision operator. The corrective factor K accounts for effects neglected in the one-dimensional analysis such as pitch angle scattering and perpendicular velocity space flattening in the resonant region. By solving the stationary two-dimensional Fokker-Planck equation numerically, Karney and Fisch found that $K = 0.39$ for $Z_i = 1$ [8]. In general the value of K is quite sensitive to Z_i because at high Z_i, the flattening in perpendicular velocity is greater. At $Z_i = 3$ and 5, $K \simeq 0.28$ and 0.23 respectively [8]. Thus, less power is required to generate current than predicted by one-dimensional analysis. In a separate study conducted at General Atomics, the time-dependent two-dimensional Fokker-Planck equation is solved numerically [3]. This study also found that for times long compared to the turn-on time, the two-dimensional code predicts more current per power dissipated than the one-dimensional result [3]

The quantity J/P_D indicates the effectiveness of current generation by rf wave. Equations (6) and (10) show that J/P_D is independent of T_e, inversely proportional to n_e, and varies rather rapidly with the phase velocity of the rf wave. High phase velocity waves are more effective in driving current, as is evident from J/P_D versus $n_{z2} = ck_{z2}/\omega$ plot of Fig. 3. However, the absolute amount of current generated is very small if the phase velocity is much larger than the electron thermal velocity. The width of the rf wave spectrum also affects J/P_D. For fixed $n_{z1} = c/u_1 v_{Te} = ck_{z1}/\omega$, a broader spectrum (larger $\Delta n_z = n_{z1} - n_{z2} > 0$) will lead to higher J/P_D. However, the value of the

parallel refractive index of the wave is limited in a plasma by accessibility criteria among other constraints. In present day tokamak plasmas with $T_e \sim 1$ KeV, rf waves with $n_z \sim 5$ will be used to generate current. Accessibility conditions will not pose a serious problem and broad rf spectra can be used. The situation is very different in reactor type plasmas. At $T_e > 10$ KeV, rf waves with $n_z \leq 2$ will be required for current drive. In this case the accessibility criteria which determine the minimum value of n_z allowed in a plasma will pose a serious constraint. Fig. 3 shows that a narrower rf spectrum will lead to higher J/P_D. It will be shown below that rf waves with very narrow rf spectra will be required to generate currents in reactors.

In high temperature reactor plasmas; e.g., $T_e = 18$ KeV, $u_1 = 2.5$, $u/c = 0.51$, electrons may become relativistic. Relativistic effects will be more important for tail electrons with $u > u_2 > u_1$. Relativistic effects are not included in the present study. However, to fully investigate the feasibility of steady state tokamak reactors driven by lower hybrid waves, a relativistic quasi-linear theory calculation must be carried out because it will provide additional correction factors to the J/P_D value. As relativistic effects will not be important in present day rf current drive experiments with relatively low temperature plasmas, scaling theories will be required to use available data in feasibility studies of rf driven steady state tokamak power reactors.

2.2 EXPERIMENTS ON CURRENT GENERATION BY LOWER HYBRID WAVES

Until recently, experimental evidence for rf driven steady state current has been non-existent. However, during the past year there have been two reports on the experimental observation of transient current generated by electron Landau damping of unidirectional hybrid waves [9,10].

An eight-ring slow wave structure was used in the Princeton L-3 linear device to generate pulsed unidirectional waves [9]. With adjacent rings phased at 90^0 with respect to each other, 85% of the rf power propagates in one direction. The wave generated current was found to be directly proportional to the power level of the rf pulse. With 17 watts of rf power, 35 mA of current has been generated. In this experiment, resonant electrons left the plasma through the end of the linear machine in a time shorter than the collision time, thus the quasi-linear plateau of the electron distribution function has not been established [9].

An rf current drive experiment has also been carried out in the General Atomic Octopole run in a divertor tokamak mode. Upon application of 5 msec pulses of up to 33 kW of rf power, a significant increase in the time derivation of the current dI/dt was observed when the rf wave traveled in the same direction as the inductively driven electron flow. When the rf wave traveled counter to the electron flow, a decrease in dI/dt was observed. With a central electron temperature of 25 eV, an estimated current

of 370 Amp was generated by an rf power of 15 KW [10]. In this experiment, however, the direction of wave propagation was controlled by the direction of the toroidal field rather than the antenna phasing. This observed phenomenon has not been explained. Also, the interpretation of experimental results was complicated by the fact that rf heating of the bulk temperature lowered the bulk resistance, causing an increase plasma current [10].

The feasibility of generating steady state current by rf waves for toroidal plasma confinement remains to be proven in toroidal plasma experiments. Several such experiments are under way or being planned [11-13].

Toroidal current generation by lower hybrid waves will be carried out in Versator II tokamak at MIT. A six waveguide array with continuously variable phase difference has been constructed. In the current drive experiment, an 800 MHz wave with a spectrum of $n_z = 6 - 12$ will be used. For initial parameters of $T_e = 275$ ev, $n_e = 2 \times 10^{13}$ cm $^{-3}$, $I_p = 40$ KA, and absorbed rf power of 75 Kw, an additional toroidal current of 20 KA is expected according to recent transport code calculations. Preliminary experimental results are expected in a few months [11].

In an experiment planned at the Argonne National Laboratory, an rf wave with a pulse length short compared to the heating time will be used to generate current. By using a short wave injection

time the complication of current increase due to rising plasma temperature can be avoided [12].

Another rf current generation experiment is being planned for the PLT tokamak in Princeton. A six waveguide array will be capable of delivering up to 1 MW of 800 MHz wave power in 500 msec pulses. Assuming only 1/16 of the microwave power will be effective in generating current, due to uncertainties in wave-plasma coupling, a current change of $\sim$ 140 KA is expected. This experiment has the option of using more waveguide units to lower the rf wave power flux in case non-linear effects occur. This may be the definitive experiment to test the feasibility of rf current generation. However, it is not scheduled before the fall of 1980 [13].

3. LAUNCHING AND PROPAGATION OF LOWER HYBRID WAVE

In this chapter we will examine these problems drawing information from existing theories as well as from available experimental data. The propagation model to be used in subsequent analysis will also be described.

3.1 PHASED WAVEGUIDE ARRAYS

The frequency of rf waves to be used for current generation is of the order of a few gigahertz. The free space wavelength of these waves is in the decimeter range so that open-ended waveguide structures (grills) can be used to launch the microwave into the plasma. The waveguide array method is desirable because it avoids coils or antennas inside the vacuum chamber. The vacuum window can be placed behind a waveguide bend so that it will not be subjected to neutron bombardment.

The launching grill consists of an array of properly phased rectangular waveguides. This system has been studied in detail theoretically by Brambilla and others [14-16]. In general, the first peak in the rf spectrum is given approximately by [17].

$$n_z \simeq cN \, \Delta\phi/\omega L \qquad (11)$$

where N is the number of waveguides in the array, $\Delta\phi$ the phase difference between adjacent waveguides, and L the total width of the array parallel to the toroidal field direction. The rf wave spectrum is narrower with increasing N. The relative phasing $\Delta\phi$ can be adjusted so that a unidirectional wave is launched.

The grill system and the Brambilla theory have been tested in several experiments. In the experiments on Princeton's H-1 linear device and ATC tokamak, waveguide-plasma coupling efficiency of 90% was obtained without the aid of any matching devices [17, 18]. The H-1 experiments were carried out with several waveguide designs. With a quadruple waveguide array, a nearly unidirectional wave with 5 dB asymmetry between upstream and downstream power was launched when $\Delta\phi = 60^0$. Another important practical result of this experiment was the lack of sensitivity of the reflection coefficient with respect to the plasma density gradient. The H-1 observations agreed quantitatively with the Brambilla theory. In the ATC experiments [18] with a double waveguide, however, only gualitative agreement with the Brambilla theory was obtained. There was no quantitative agreement with theory for reflection as a function of $\Delta\phi$. In the Alcator A experiments [19] with a double waveguide, results of transmission as a function of $\Delta\phi$ were qualitatively different from theoretical predictions when the power flux

exceeded 1 KW/cm^2. Results similar to Alcator A were obtained in experiments on the JFT-2 tokamak [20,21]. With a four-waveguide array system, it was found that the rf wave spectrum within the plasma was not controlled by $\Delta\phi$ variation when the power flux exceeded 0.5 KW/cm^2 [20]. The Alcator A and JFT-2 results were interpreted in terms of nonlinear effects [19, 21]. The effect of possible nonlinear processes to the current driving scheme will be discussed in more detail in section 3.3.

All presently available experiment data were obtained with waveguide arrays consisting of four elements or less, (a six waveguide array will be used in the Alcator C and PLT lower hybrid experiments). To generate current in tokamak reactors, however, arrays consisting of fourteen to twenty elements will be required because of the narrow wave spectrum necessary for current driving purpose ($n_z \sim 1.5$, $\Delta n_z \sim 0.3$). Effects of the finite size of the partition dividing the waveguides, and possible coupling between different waveguide arrays warrant further study.

3.2 PROPAGATION OF LOWER HYBRID WAVE

Properties of lower hybrid waves have been studied extensively both theoretically [22, 23], and experimentally in linear [24] as well as toroidal [25] machines. Various lower hybrid heating experiments [18-20, 26, 27] have also provided confirmation of the linear theories.

A slow wave launched by a waveguide array under ideal conditions propagates in a well defined resonance cone in the r-z direction towards the plasma center. The distance traveled in the axial (z) direction is approximately of the order of $r(m_i/m_e)^{1/2}$ [23]. In the current driving scheme the frequency of the wave will be greater than the lower hybrid frequency anywhere in the plasma, so that there will be no resonance layer.

Under the cold plasma electrostatic model, the dielectric function of the slow wave is given by

$$\varepsilon_R(k,\omega) = 1 - \frac{\omega_{pe}^2}{\omega^2 - \Omega^2}\left(\frac{k_\perp}{k}\right)^2 - \left(\frac{\omega_{pe}}{\omega}\,\frac{k_z}{k}\right)^2 - \left(\frac{\omega_{pi}}{\omega}\right)^2 \qquad (12)$$

where $k^2 = k_\perp + k_z^2$. Setting $\varepsilon_R = 0$ yields the dispersion relation

$$\omega^2 = \frac{1}{2}\left\{\omega_{UH}^2 - \left[\omega_{UH}^4 - 4\Omega_e^2\,\omega_{pi}^2\left(1 + \frac{m_i}{m_e}\,\frac{k_z}{k}\right)\right]^{1/2}\right\} \qquad (13)$$

which gives the Trivelpiece - Gould mode ($\omega = \omega_{pe}\,k_z/k$) at the plasma edge where $\omega \sim \omega_{pe}$. At the plasma center where $\omega << \omega_{pe}$, Eq. (13) gives the lower hybrid wave, dispersion relation

$$\omega^2 = \omega_{LH}^2\,(1 + m_i k_z^2/m_e k^2) \qquad (14)$$

where $\omega_{LH}^2 = \omega_{pi}^2/(1 + \omega_{pe}^2/\Omega_e^2)$ and $\omega_{UH}^2 = \omega_{pe}^2 + \Omega_e^2$. The perpendicular group velocity is

$$|v_{g_\perp}| = \omega_{pe}^2\Omega_e^2\,k_\perp k_z^2/k^4\omega\omega_{UH}^2 \qquad (15)$$

where

$$k_\perp = k_z(-\varepsilon_3/\varepsilon_1)^{1/2}$$

$$\varepsilon_3 = 1 - (\omega_{pe}/\omega)^2$$

$$\varepsilon_1 = 1 + (\omega_{pe}/\Omega_e)^2 - (\omega_{pi}/\omega)^2 \ .$$

The parallel refractive index of the slow wave must be higher than a critical value or it will be converted into the outward propagating fast wave [28,29]. The fast wave is reflected at the critical layer and trapped as surface waves in the plasma. In the ATC experiments, for example, only 77% of the wave energy coupled into the plasma via a double waveguide penetrated deep into the plasma [18]. Such surface waves are undesirable for current generating purposes. The accessibility conditions are given in terms of n_{LC}, the lower cut off value of the parallel refractive index of the slow wave,

$$n_z > n_{LC} = (1 - \omega^2/\Omega_e\Omega_i)^{-1/2} \qquad \omega \leq \omega_c \qquad (16a)$$

$$n_z > n_{LC} = \omega_{pe}/\Omega_e + [1 + (\omega_{pe}/\Omega_e)^2(1 - \Omega_e\,\Omega_i/\omega^2\,)]^{1/2}, \quad \omega > \omega_c \qquad (16b)$$

where $\omega_c^2 \equiv (\omega_{pe}^2\Omega_i/2\Omega_e)\,[\,(1 + 4\Omega_e^2/\omega_{pe}^2)^{1/2} - 1]$. If ω in Eq. (16a) is replaced by the lower hybrid frequency, ω_{LH}, then Eq. (16a) becomes $n_z > (1 + \omega_{pe}^2/\Omega_e^2)^{1/2}$ which is the accessibility condition used in Refs. [2] and [4]. This condition is incorrect in the context of the present problem because there will be no lower hybrid resonance layer in the plasma.

As the lower hybrid wave travels into the hot plasma center, it may suffer linear mode conversion into into heavily damped hot ion waves [30]. This process may be favorable for the purpose of lower hybrid heating because it effectively transfers wave energy to the ions, but it is clearly unfavorable for current generation. To avoid linear mode conversion, we require that n_z be less than an upper cut off value n_{UC} [30]

$$n_z < n_{UC} = \frac{c}{2v_{Te}} \left(\frac{\omega^2}{\omega_{pi}^2} + \frac{\omega^2}{\Omega_e \Omega_i} - 1 \right) \left(\frac{3}{2} \frac{T_e}{T_i} + \frac{3}{8} \frac{\omega^4}{\Omega_e^2 \Omega_i^2} \right)^{-1/2} \qquad (17)$$

To satisfy Eqs. (16) and (17) simultaneously imposes a minimum value on the frequency of the lower hybrid wave, i.e., $\omega > \omega_{min}$. For typical parameters of interest in reactor plasmas $\omega_{min} \sim 1.4 - 1.7\ \omega_{LH}(\phi)$. Figure 4 plots n_{LC} and n_{UC} as a function of plasma radius assuming parabolic density profile and $\omega = 2\omega_{LH}(\phi)$. As can be seen, there is a window of n_z accessible to the plasma center. This window will be considerably narrower or even disappear if lower frequency is used.

As the wave propagates in the plasma, it will suffer electron Landau damping, i.e., power is dissipated to generate current. With a Maxwellian electron distribution, the wave will be completely damped in a short distance if $n_z T_e^{1/2}(\text{KeV}) \gtrsim 5$. However, the quasi-linear plateau will be raised in a time of the order of collision time

$\tau_c = m_e^2 v_z^3/[4\pi(z_i + 2)n_e e^4 \ell n\Lambda]$. In the steady state, the rf wave power flux will decrease by one half over a distance

$$L_{1/2} = S/2P_D \tag{18}$$

where $S = |v_{g_\perp}|\mathcal{E}$ is the wave power flux. Thus, for the wave to reach the plasma center without being completely dissipated, it is required that

$$n_z < n_{LD} \simeq cu_1/v_{T_e}u_2C_p \tag{19}$$

$$C_p = \left\{\ell n[7\times10^3\ n_{20}^2\ T_e^{-1/2}\ \ell n(u_2/u_1)a/S]\right\}^{1/2}$$

where the plasma radius a is in meters and S is in MW/m^2.

Decay of the lower hybrid wave via various types of parametric instabilities may also occur. Besides transferring energy to the heavily damped ion quasi-modes, parametric instabilities would also greatly distort the lower hybrid wave spectrum, and thus have to be avoided for current generation purpose. It has been shown that for tokamak-like plasmas, the parametric instability with greatest growth rate occurs for rf frequencies in the range of $1 < \omega/\omega_{LH}(\phi) < 2$ [31]. In the ATC lower hybrid heating experiments, parametric instabilities in the bulk plasma were observed only for $\omega/\omega_{LH}(\phi) < 1.9$ [32]. Therefore, to avoid parametric instabilities in the bulk plasma, we pick the rf wave frequency to be twice the

central lower hybrid frequency $\omega_{LH}(\phi)$. However, this may not prevent parametric instabilities occurring at the plasma surface as will be discussed in the next section.

The various regions for wave-plasma interaction described above are depicted in Fig. 5. We see that n_{LC} decreases with higher B, while n_{UC} decreases with higher T_e as given in Eqs. (16) - (17). Since electron Landau damping is the mechanism responsible for current generation, we choose the operating rf frequency to be in that region.

The parameter n_z is very important in determining current generation efficiency as is apparent from Fig. 3. In slab geometry, n_z is a constant for propagation into a perpendicular density gradient. However, in toroidal geometry, n_z varies because it is coupled to other components by the curved magnetic field lines [33]. In general, the variation of n_z is complicated, and must be carefully taken into account in designing reactor current drive. Since n_z is usually barely greater than n_{LC} for reactor current drive, any downshift of n_z will result in the inaccessibility of the wave. For the present study, however, the reference parameters ($B_o \sim 7.5$ T, $n_e \sim 10^{20}$ m^{-3}) are such that $\omega_{pe}/\Omega_e < 1$. In this high toroidal field configuration the poloidal contribution to the variation of n_z is negligible, and we can approximate [33]

$$n_z(r) = n_z(a)(R + a)/(R + r) \tag{20}$$

where $n_z(a)$ is taken at the outer edge of the torus where B_o is lowest.

3.3 NONLINEAR EFFECTS

Many nonlinear effects may occur in the plasma in the presence of a strong wave [34]. It has been observed experimentally that density fluctuations of the plasma [35] can focus the lower hybrid resonance cone azimuthally and modulate its radial location [36].

Edge plasmas are especially susceptible to nonlinear effects because of their low density and temperature. It has been shown theoretically that at high intensity the waveguide-plasma coupling can no longer be predicted by the Brambilla theory. Instead, both the reflection coefficient and the spectrum launched will be functions of the wave intensity [37]. Furthermore, when the oscillating velocity v_o of the resonant electrons in the rf field is large so that they become trapped, electron Landau damping will be radically modified. In such case the quasi-linear theory of section 2.1 is no longer valid [37]. Resonant electrons will be trapped if [37]

$$\omega_B \equiv (eEk/m)^{1/2} >> \gamma_L \tag{21}$$

where ω_B is the bounce frequency, E the electric field and γ_L is given in Eq. (8) with D = 0. The parameter γ_L/ω_B is plotted in Fig. 6 for f = 2.8 GHz, S = 0.5 KW/cm^2, n_z = 1.5, B_o = 7.5 T.

Another nonlinear effect, parametric instability, has been observed in many tokamak experiments. In both the ATC [32] and the Wega [26] lower hybrid heating experiments, ion heating were only observed accompanied by parametric decay spectra. Parametric instabilities were also reported in the Alcator A [19] and JFT-2 [21] lower hybrid heating experiments. Parametric instabilities are deleterious to rf current drive in several ways. First, it may cause unwanted energy deposition in the plasma surface. Second, it transfers wave energy to the ions which carry little current. Third, it may destroy the unidirectionality of the lower hybrid wave crucial for current generation. Fourth, it may cause a large shift in $k_z = n_z\omega/c$. The last two effects are apparent from the frequency and wave vector matching conditions for parametric decay processes

$$\omega_o = \omega_1 + \omega_2; \quad \vec{k}_o = \vec{k}_1 + \vec{k}_2 \tag{22}$$

where the subscript o refers to the original wave, and 1,2 refer to the daughter waves. Equation (22) has been verified in many experiments [38]. In typical cases, the k-vectors of the two daughter waves point in nearly

opposite directions. The daughter waves may still be able to penetrate into the plasma and contribute to heating, but a large shift in the n_z of the daughter wave such as that observed in Alcator A [19] greatly reduce the effectiveness of the current driving scheme.

Lower hybrid waves inside a plasma can excite a host of parametric instabilities [36]. Near the plasma center where $\omega/\omega_{LH} < 2$, nonresonant decay into ion quasi-modes may occur [40]. This was the effect observed in ATC and Wega [20,32]. According to these experiments, this instability can presumably be avoided by choosing the rf frequency such that $\omega/\omega_{LH} \geq 2$ everywhere in the plasma. At the edge of the plasma where $\omega/\omega_{LH} >> 1$, resonant decay into cold lower hybrid wave and ion-acoustic wave or ion cyclotron wave may occur [31]. This has been identified as the decay process observed in JFT-2 [21]. The convective threshhold power per grill above which resonant decay will be excited a unidirectional wave is given by [31]

$$P_{th} = \frac{1.9 \times 10^4}{n_z} \frac{L_y}{L_z} \left(\frac{m_i}{m_e}\right)^{1/2} \frac{\omega}{\omega_{pi}} \frac{B^2 C_s^2}{c^2 k^2} \left(1 - \frac{\omega_{LH}^2}{\omega^2}\right)^{3/2} Q_c \quad (W) \tag{23}$$

$$Q_c = \frac{\sqrt{\pi}\,\omega}{k_z v_{Te}} \left\{ 1 + \left(\frac{T_e}{T_i}\right)^{3/2} \left(\frac{m_i}{m_e}\right)^{1/2} I_1(b_i) e^{-b_i} \exp\left[- \left(\frac{\omega - \Omega_i}{k_z v_{Ti}}\right)^2 \right] \right\}$$

where L_y, L_z are the dimension of the waveguide in y and z directions, $\omega_{pi}^2 = 4\pi n_e e^2/m_i$, $C_s^2 = T_e/m_i$, $v_{Ti}^2 = 2T_i/m_i$, $\Omega_i = eB/m_i c$, $b_i = (k_\perp v_{Ti}/\Omega_i)^2/2$, and I_l is the modified Bessel function. The threshhold depends on the plasma edge parameters. Using parameters relevant to the reference reactor of the study, i.e., B = 6T, n_z = 1.6, f = 2.86 Hz, L_y/L_z = 2.5, $T_e = T_i$ = 1 KeV, $n_e = 10^{19} m^{-3}$, a threshhold value of $P_{th} \tilde{-}$ 9MW is predicted by Eq. (23). The total rf power required to drive the reference steady state reactor is approximately 60 MW in the ideal situation. Thus it appears that resonant decay instability may be avoided by distributing the input power into eight or more port units.

4. CHARACTERISTICS OF NEARLY IGNITED PLASMAS

At ignition, the electron and ion energy equations are given by:

$$(1 - G_i)P_\alpha + P_D - P_{ec} - P_{cyc} - P_{br} - P_{ei} = 0 \tag{24}$$

$$G_i P_\alpha - P_{ic} + P_{ei} = 0 \tag{25}$$

where P_{ec}, P_{cyc}, P_{br}, P_{ei}, and P_{ic} denote electron transport loss, cyclotron radiation loss, bremsstrahlung loss, electron-ion energy equilibration loss, respectively. P_{ec} is determined by the empirical scaling law time [41] and P_{ic} is determined by the neo-classical confinement time. P_α is the alpha power density produced by fusion. G_i is the fraction of alpha energy transferred to the ions.

$$P_{ec} = 0.69\ T_e/a^2 \tag{26}$$

$$P_{ic} = 0.27\ (n_{20}/I_p)^2\ (T_i/A) \tag{27}$$

$$P_{cyc} = 5.88 \times 10^{-10} n_{20}^{1/2}\ B^{5/2}\ T_e^{11/4} \tag{28}$$

$$P_{ei} = 1.83\ n_{20}^2\ (T_e - T_i)/T_e^{1.5} \tag{29}$$

$$P_{br} = 7.1 \times 10^{-3}\ n_{20}^2\ T_e^{1/2} \tag{30}$$

$$G_i = (2/x)\{\ell n[(1 + x - \sqrt{x})/(1 + \sqrt{x})^2]/6 + \tan^{-1}[(2\sqrt{x} - 1)/\sqrt{3}]/\sqrt{3} + 0.3\} \tag{31}$$

where $x = 106.9/T_e$. All temperatures are in KeV, B in T, power density in MW/m^3, current in MA. Parabolic density and temperature distributions were assured.

For a given average electron temperature $\bar{T}_e$, the ion equation (25) can be solved for $\bar{T}_i$, then the electron equation (24) is solved to give the minimum density required for ignition, $\bar{n}_{ign}$. The minimum current required for confinement is determined by MHD stability consideration. If the maximum allowable poloidal beta is given by $\beta_p \leq A = R/a$, then

$$I \geq I_p = acS\,[2\pi\bar{n}_e(\bar{T}_e + \bar{T}_i)\,/\,A(1 - \Gamma_\alpha)]^{1/2} \qquad (32)$$

where c is the speed of light and $\Gamma\alpha$ is the ratio of alpha pressure to the thermal plasma pressure

$$\Gamma_\alpha = -.0613 + 1.2\times 10^{-2}T_e + 5\times 10^{-5}T_e^2 + 2.5\times 10^{-6}T_e^3 . \qquad (33)$$

The current generated must also be able to confine the alpha particles. Theory predicts that in order to confine the alphas, the product of current and aspect ratio, IA, must exceed a certain value [42]. A rough estimate of this value for a circular plasma is IA > 7.5 MA [42]. (In all cases considered for the study, this condition is satisfied.)

Figure 7 plots $\bar{T}_i$ and $\bar{n}_{ign}$ as a function of $\bar{T}_e$ for R = 6m, A = 5, B_o = 7.5T. Two processes for alpha slowing down are considered. The curves marked "C" give the result for the classical mode in which classical slowing down time for the alphas [43] has been used. In the classical mode given by Eqs. (31) and (33), $0.1 \leq G_i \leq 0.4$ [44] and $0 \leq \Gamma_\alpha \leq 0.3$ for $5KeV \leq \bar{T}_e \leq 30$ KeV. The curves marked "A" give the result for a possible mode in which the alphas are slowed down anomalously via velocity space instabilities [45].

In this case it is assumed that the alpha slowing down time is much less than the classical slowing down time. In addition, most of the alpha energy will be deposited in the ions so that $G_i \simeq 1$ and $\Gamma_\alpha \simeq 0$. The anomalous transfer of alpha power to ions facilitates ion-electron temperature decoupling, i.e., $\bar{T}_e << \bar{T}_i$, which is favorable for current generation.

The plasma density is limited by the ignition criterion on the one side and the plasma pressure on the other, $\bar{n}_{ign} \leq \bar{n}_e \leq \bar{n}_{max}$, with

$$\bar{n}_{max} = \bar{\beta}_t B_o^2 / 8\pi [(1 + \Gamma_\alpha)\bar{T}_e + \bar{T}_i] \qquad (34)$$

where $\bar{\beta}_t$ is the averaged ratio of the plasma kinetic pressure to the magnetic field pressure.

5. CURRENT GENERATION EFFICIENCY IN A TOKAMAK REACTOR

An important figure of merit for an rf-driven tokamak reactor is:

$$Q \equiv P_F/\overline{P}_D = 1.25\ E_\alpha \overline{n}_e^2 \langle\sigma v\rangle_{DT} \left[2 \int_0^1 P_D\ \rho d\rho \right]^{-1} \qquad (35)$$

where E_α = 3.5 MeV, $\langle\sigma v\rangle_{DT}$ is the average fusion cross-section, $2\pi^2 R\overline{a^2 P_D}$ is the rf power required to generate I_p. In this chapter we systematically study the variation of Q with various plasma parameters.

We pick the parameters of the high field demonstration power reactor HFCTR [5] as our reference set, R = 6m, a = 1.2m, B_o = 7.5 T, $n_e = n_{eo}(1 - \rho^3)$, $T_e = T_{eo}(1 - \rho^2)$, $T_i = T_{io}(1 - \rho^2)$. We will use in our model $B_t = B_o(1 + \rho/A)$. The deuterium-tritium mixture is 50-50 and Z_{eff} is taken to be 1. With fixed R, A, $\overline{n}_e$, $\overline{T}_e$, and B_o, plasma elongation increases I_p, but it also increases the plasma cross section, so that the current density J remains approximately constant. Since Q is determined by the current and power densities, plasma elongation will have little effect on the value of Q. Therefore, we will consider a circular reactor when investigating the effects of plasma parameters on Q. Plasma shape factors will be taken into account when we consider total fusion power of the reactor.

5.1 CENTRALLY PEAKED CURRENT PROFILE

For a given $\bar{T}_e$ and $\bar{n}_e$, the value of Q varies with the plasma profiles. Table 1 shows the effect of density, temperature and current profiles on Q. In general, a more peaked profile will yield a lower Q. Since $J/P_D \propto 1/n_e$, more gradual density and current profiles mean there are more electrons at the low density region to carry current effectively, thus leading to higher Q. By the same argument, it can be seen that much less rf power is required to generate the surface currents proposed in Ref. 4. In fact, we find that as much as a factor of 1.5 improvement in Q over a parabolic current profile can be obtained if all current is generated in the $\rho = r/a > 0.7$ region. However, because of the question of the stability of surface currents, we have only considered centrally peaked current profiles in this study.

To demonstrate centrally peaked current profiles can be generated by lower hybrid waves when essential propagation characteristics are taken into account, we have solved Eq. (17) numerically for numerous boundary conditions. The incident wave power flux and spectral shape are taken as variables. The wave spectrum is then divided into 100 divisions each of the form of Eq. (3). Accessibility constraints and n_z variation are included in the design. One of the best results is shown in Fig. 8. Figure 8 depicts the variation of the

lower hybrid wave spectrum as it propagates into a plasma with parabolic density and temperature profiles. The dotted curve in Fig. 8 gives n_{LC}, according to Eq. (16), and the spectral peak is seen to shift to higher n_z according to Eq. (20). The initial increase in $\mathcal{E}_{kz}$ is due to the decrease in $v_{g_\perp}$ as n_e increases with $(1 - \rho)$. The decrease of $\mathcal{E}_{kz}$ near the plasma center is due to Landau damping of the wave. The portion of power flux which reaches the plasma center without being absorbed continues propagating and suffers further damping. Eventually, a small portion may emerge unabsorbed from the plasma and is either lost or reflected at the wall. As can be seen from Fig. 8, in order to generate current effectively, a very narrow rf spectrum is required. This would demand careful waveguide design.

The rf wave driven current profile is depicted in the insert, which is centrally concentrated except for a slight depression in the middle. To generate enough current for MHD stability with this particular rf wave spectrum and plasma parameters, 3.3% of the fusion power has to be regenerated as dissipated rf power, i.e., Q = 30. This value of Q does not take into account the small portion of the wave spectrum which is reflected due to mode conversion to fast waves. Thus a reasonable current profile can be generated by lower hybrid waves with a reasonable spectrum. With the same plasma parameters, different rf spectra will generate

very different current profiles. For example, a broader spectrum with less spectral intensity will result in surface current profile with higher Q value.

5.2 PARAMETER STUDY

The value of Q as a function of various plasma parameters will be examined for a parabolic current profile

$$J = J_o(1 - \rho^2) \tag{35}$$

$$2\pi\overline{a^2} = \int J \, \rho d\rho = I_p \tag{36}$$

Although one may not be able to find a wave spectrum that will generate an exactly parabolic current profile, we have shown in the last section that while simultaneously taking into account wave propagation effects, a centrally peaked current profile can be generated with $Q \sim 30$. Fixing a hypothetical current profile allows a systematic examination of current generating efficiencies.

The following procedure is used. For a set of plasma parameters, the local current density is determined by Eqs. (35)-(36). By setting $\omega = 2\omega_{LH}(0)$, $n_{z2} = n_{LC}$ in Eq.(6) we can find n_{z1} as a function of ρ and then use Eqs. (10) and (33) to determine Q. Since the maximum of n_{LC} usually occurs at some position $\rho_m \neq 0$, we have let $n_{LC}(\rho < \rho_m) = n_{LC}(\rho_m)$ to insure correct accessibility. In most cases the value of n_z lies in the range $1.2 \lesssim n_z \lesssim 2.0$. Typically,

$n_{z1}/n_{z2} \sim 1.06 - 1.2$. Thus, a very narrow rf spectrum is required for current generation, in agreement with the case depicted in Fig. 8.

We have assumed that the rf wave will propagate radially inward from the low magnetic field side of the minor cross section. In general, if we assume wave propagation in the high magnetic field side, i.e., $B_t = B_o/(1-\rho/A)$, Q will increase by $\sim$ 15%. In reality, the rf wave spirals in following the resonance cone and passes through both the high and low magnetic field sides before reaching the center. However, this complex propagation behavior is not taken into account in our model as discussed in Section 2.1. We will adopt the lower Q values obtained with $B_t = B_o(1 + \rho/A)$ in this study.

Since n_{LC} increases with rf wave frequency $f = \omega/2\pi$, Q decreases with f. The dependence of Q on f is depicted in Fig. 9, where the circles mark the minimum f required for penetration into the plasma center as determined by accessibility and linear mode conversion. The crosses in Fig. 9 mark where f equals twice the center lower hybrid frequency. We have picked $\omega = 2\omega_{LH}(0)$ in order to avoid parametric instability. Higher Q can be achieved if lower frequencies can be used. Classical alpha slowing down time is used. (Except for the dashed curve of Fig. 11, all results presented in this paper are for the classical mode).

The variation of Q with the parallel index of refraction of the wave is shown in Fig. 10. The rapid decline of Q as n_{2z} increases is expected by inspecting Fig. 3. It is obvious that the wave spectrum inside the plasma must be well under control for the current drive scheme. An upshift in n_z will lead to a large drop in Q, a downshift in n_z may lead to inaccessibility of the wave to the plasma center. For this reason alone, current generation by lower hybrid wave will be more difficult to achieve than lower hybrid heating of the plasma.

Figure 11 shows Q as a function of $\bar{T}_e$. The initial rise of Q with $\bar{T}_e$ comes from the rapid increase of P_F with $\bar{T}_i$. The drop of Q with higher $\bar{T}_e$ is caused by the gradual saturation of P_F at high $\bar{T}_i$ coupled with the required increase of I_p with $\bar{T}_e$. The maximum Q for the classical mode occurs at around 15-18 KeV. This Q versus $\bar{T}_e$ behavior agrees qualitatively with Ref. 4. The maximum Q obtained in the anomalous mode is $\sim$ 10% more than the maximum Q for the classical mode. This can be explained in terms of the former's higher $\bar{T}_i$ for more fusion power and lower $\bar{T}_e$, $\bar{n}_{ign}$ for lower I_p. Since the anomalous alpha slowing down time is not experimentally verified, we selected the lower value of Q resulting from the classical alpha-slowing-down time.

The fusion power P_F scales as n_e^2. The rf power required to generate sufficient current for MHD stability, $P_D I_p/J$, scales as $n_e^{3/2}$. However, the actual variation

of Q with $\bar{n}_e$ as shown in Fig. 12 is much slower than $n_e^{1/2}$. This is due to the implicit dependence of Q on $\bar{n}_e$ through accessibility criteria.

From the discussion of Section 3, we see that n_{LC} decreases with higher magnetic field, thus higher Q can be achieved with larger B_o. Figure 13 depicts the variations of n_{LC} and Q with B_o for several reactor sizes. Equation (32) shows that the current density required for MHD stability decreases for the larger plasma cross-sectional area, $J_p = I_p/\pi\overline{a^2} \propto \sqrt{A}/R$. Since Q is mainly determined by current and power densities, larger reactors (i.e., larger major radius designs) are expected to result in lower current densities and higher Q values. In order to achieve a specific Q value, a trade-off between larger reactor size and higher magnetic field at plasma can be made, as is shown in Fig. 14. From the above discussion it follows that for fixed $\bar{T}_e$ and $\bar{n}_e$, Q decreases quite rapidly with $\bar{\beta}_t = 8\pi\bar{n}_e(\bar{T}_e + \bar{T}_i)/B_o^2$ as depicted in Figure 15.

The total fusion power of a reactor can be increased by increasing $\bar{n}_e$, R, a, or plasma elongation. While elongation leaves Q essentially unchanged, larger $\bar{n}_e$ and R both enhance Q. The dependence of Q on aspect ratio is more complex. For a fixed magnetic field at toroidal coils B_{To}, the field at plasma axis B_o increases with increasing A. This will enhance Q as is apparent from Fig. 13. On the other

hand, Eq. (32) shows that current density required for MHD stability goes as $A^{1/2}$, and for fixed $\bar{T}_e$, $\bar{T}_i$ will be less in reactors with larger A. Both of these effects will decrease Q with increasing A. Figure 16 depicts the total fusion power and Q as a function of the aspect ratio of a reactor with R = 6 m, S = 1.5 and B_{To} = 13 T. The field at the plasma axis is $B_o = B_{To}(1 - 1/A - d/Aa)$, where the distance from plasma edge to the toroidal coils, d, is taken to be 1.4 m. By varying A from 3 to 5, Q changes by less than ten percent. Thus, high power density reactors can be achieved by going to smaller A and larger $\bar{n}_e$, with limits imposed by wall loading and plasma pressure considerations only.

The design parameters of a 2500 MW reactor with Q = 40 are given in Table 1. The lower hybrid wave spectrum necessary to provide this Q is given in Fig. 17 as a function of radial position.

5.3 DISCUSSION

The values of Q in section 5.2 were obtained using several assumptions. These assumptions are discussed below.

(1) The wave propagates in from the low magnetic field side of the torus. The value of Q may increase by an estimated 5 - 7% if wave propagation through both high and low magnetic field regions are taken into account.

(2) A purely unidirectional lower hybrid wave is assumed. Any residue wave flux traveling in the opposite direction will reduce Q.

(3) An optimum wave spectrum is assumed everywhere inside the plasma. This is clearly idealistic. By comparing the results of sections 5.1 and 5.2, a $\sim$20% reduction in Q is expected if the rf wave spectrum is fixed at the boundary only instead of everywhere in the plasma.

(4) The power loss due to waves reflected as fast waves is neglected. The value of Q will be reduced if these losses are taken into account.

(5) A parabolic current profile is assumed. Q will be larger for a more gradual current profile.

(6) Inspection of Eqs. (5) and (8) shows that for a wave power flux

$$S_{rf} > 10^{-3}\, n_{20}\, T_e\, f\, n_z\, \Delta n_z \qquad (W/cm^2) \qquad (37)$$

the current generated as well as the power dissipated will be essentially independent of S_{rf} (f is in GH_z). If Eq. (37) is not satisfied, power dissipation will increase rapidly due to the finite slope in the distribution function. However, in all situations considered in this study, Eq. (37) is easily achieved. On the other hand, since J and P_d are independent of S_{rf}, the only wave parameters that can be used to control the current profile are those of the wave spectrum.

(7) The present analysis is based on the assumption that $Z_{eff} = 1$. For steady state power reactors, especially for designs without a divertor, the effect of a considerable concentration of impurities and alphas must be taken into account.

6. REACTOR ENGINEERING

6.1 HIGH EFFICIENCY MICROWAVE ENERGY DELIVERY AND RECOVERY SYSTEM

The most distinctive engineering feature of the rf current-driven steady-state tokamak reactor is the continuous wave microwave power delivery system. Even after a realistic loss inventory has been made for a lower hybrid energy delivery system, overall system efficiency is high, permitting economical continuous operation of a moderate-Q plasma. Because of its high, steady-state recirculating power, the system differs from a previous design of a lower hybrid heated tokamak[46] by being designed primarily for high efficiency, rather than low initial cost.

The reference microwave circuit is shown in Figure 18. Power output from crossed-field amplifiers is sent through circulators into a copper-phased waveguide grill of the type described in Section 3.1. The reflected wave is recirculated through a direct energy recovery system. This microwave circuit includes several distinct features:

(1) The drivers that convert dc to rf power are crossed-field amplifiers (CFA) which have considerably lower gain than klystrons at the same frequency. However, the input power to CFA is not dissipated as in a

klystron, but is carried as a traveling wave to the output. Furthermore, unlike klystrons, a CFA can support a moderate amplitude, backward-traveling wave without efficiency degradation. Because of the last property, only a modest degree of protection (15 db) is required at the output circulator. Thus ferrite loss is minimized.

(2) A simple, cheap and efficient direct energy recovery system may be achieved by directing the reflected power through each output circulator into the input port of an adjacent CFA, which feeds a vertically adjacent waveguide in the plasma-coupling grill. In this way, the reflected power is not subjected to the dc-to-rf conversion inefficiency of the tubes, and it travels to the output ports nearly losslessly. Direct energy recovery compensates for the inefficiency caused by imperfect wave-plasma coupling.

(3) Sapphire windows and copper waveguides are selected as the lowest loss materials at S-band frequencies (2-3 GHz). The incremental efficiency offered by silver-coating the copper waveguide is too trivial to justify the expense.

6.1.A Benchmarks in Efficient Production of S-Band Microwave Power

Each component of the high-power microwave delivery has demonstrated high efficiency and reliability

in previously documented benchmark systems. Some benchmark values of component efficiencies are listed below.

- In 1964, Skowron and Brown[47] demonstrated a crossed-field amplifier which developed 400 kW CW at a frequency of 3,000 MHz, a gain of 9 db and an overall efficiency of 72%. The electronic efficiency of the tube, exclusive of power dissipated at the cathode, in the straps, and in circuit losses, was at least 80%.

- A zero degree cut sapphire window was shown by Goldfinger[48] to be capable of transmitting 1 MW of power at 8 GHz for 31 minutes without failure. Transmission of 35 kW/cm^2 was demonstrated by Johnson[49] with window losses of only 1.7 W/kW.

- Circulators protecting the klystrons in the Alcator C lower hybrid heating experiments provide over 35 db of isolation, with an insertion loss of only 0.23 db at C-band (4.6 GHz).[50]

- Waveguide and rectifier losses are available from manufacturer's specifications. Typical transformer and bus losses were taken from the Westinghouse Transmission and Distribution Reference Book.[51]

6.1.B Energy Inventories for Reference Design

A loss inventory of the reference design is shown in Fig. 19. The cases of no reflected power and 20%

reflected power are calculated. In the case of no reflected power, a 50% efficient delivery system could be built in the near future with previously developed benchmark components. Assuming there will be a component development program, and following a recent technical assessment[52], a CFA with an efficiency of 85% and a gain of 15 db can be projected. With these figures, a 73% efficient system is obtained. In all subsequent analyses, we assume that a successful development program will occur. The assumption is based on technical projections[52, 53] and the observation that, if the tube development program costs $2-4M and the cost of electricity is $0.3/kW-hr., the investment would be returned in a few months of operation of a single reactor.

With perfect coupling to the plasma, an overall efficiency of 73% is predicted for a developmental system. With 80% coupling and no direct energy recovery, this is reduced to 58%, but with direct recovery the overall efficiency is restored to 68%. For the reference design, with Q=40 during steady state and Q=25 for heating to ignition, this represents a recirculating power loss of 91 MW. Component ratings are shown in Table 3. Notice that the regulated dc power supplied to the crossed-field amplifier can actually be less than the rf power out, since the entire delivery system to the plasma is behaving like a large resonator.

6.2 EFFECT OF STEADY-STATE OPERATION ON REACTOR ECONOMICS

6.2.A Introduction

The benefits of steady-state operation of tokamaks over pulsed operation are difficult to quantify because of the lack of self-consistent designs to be used as the basis for comparison, as well as fundamental physics and engineering uncertainties inherent in both concepts.

The most obvious gain with steady-state operation will be the increase of averaged electrical power by a factor of inversed duty cycle. Other potential advantages associated with steady-state current drive in takamaks are:

(1) First-wall life could be enhanced through the elimination of fatigue failure. Conversely, first-wall loading could be increased for the same design life.

(2) The size of the ohmic heating transformer could be reduced.

(3) The equilibrium field coil power supplies could be derated, because they would no longer need to be rapidly pulsed during machine start-up.

(4) An expensive poloidal field system motor-generator-flywheel set would not be necessary to buffer start-up and shutdown loads from the utility line.

(5) An expensive thermal storage system, necessary to prevent excessive temperature drop in the steam generator feedwater, could be eliminated.

The steady-state system also presents several additional difficulties and potential disadvantages.

(1) Recirculating power would be high, because of the continuous auxiliary heating associated with a steady-state current drive.

(2) In so far as the current-driving rf supplies do not contribute to the bulk heating of the plasma, they would represent an additional cost.

(3) Impurity control requirements are more severe for a steady-state tokamak reactor than for a pulsed reactor.

(4) If high temperature operation is necessary to provide sufficiently high Q in a relatively compact plasma, then ripple requirements will be more severe than for a pulsed plasma.

The gains and disadvantages of steady-state operation and the trade-offs between them will be considered in more detail in the following sections. A crude estimate of the potential cost reduction for the steady-state current-driven reactor concept will be provided in the last subsection.

6.2.B First Wall Life

The effects of neutron swelling, brittle fracture, creep crack growth, and fatigue damage on first wall life

have been considered in this study following the methods of Prevenslik[54] and Mattas.[55] It is found that, while it appears obvious that lifetime and first-wall loading limitations are less restrictive for steady-state reactors than for thermally pulsed reactors, there is no obvious first-order advantage for a stainless-steel first wall operating at 450^{o} C and facing the HFCTR plasma. Nor is it clear how to extrapolate to the permissible use of significantly higher wall loadings and first-wall temperaturs, using the ORNL/Westinghouse demo blanket cooling concept.

In comparing the first wall lives of pulsed vs. steady-state operation, the effect of plasma disruptions, a question not previously considered to be relevant to first-wall design, may be the dominant life-limiting factor. This problem depends on the properties of ignited tokamak plasmas and needs much further study.

The structural integrity of structural materials in a fusion first-wall design has been studied by Prevenslik[54] for the ORNL/Westinghouse demo blanket design study[56] and parametrically by Mattas and Smith[55] as part of the Tokamak Power Plant Systems Program at Argonne. A study by Meyer[57] concluded that, over a broad range of wall loadings, steady state fusion reactors could support nearly twice the wall loading

as 500 s-cycle pulsed reactors. Meyer's technique used fatigue damage analysis, neglecting swelling, brittle fracture, and creep crack growth. All of these were included in the above-mentioned studies by Prevenslik and Mattas, whose methods are in rough agreement, where they coincide, and will be used in this discussion.

Prevenslik analyzed a first wall design, believed at this time to be near optimal, for the case of a 10^5 pulse design life, 4 MW/m^2 neutron wall loading, a lithium blanket, helium cooling and a stainless-steel structure. The most limiting factor was excessive deformation, due to neutron swelling, with a safety margin of only 1.28 before the cooling gap is increased by 30% For the reference case, the cooling channel gaps were fairly small, only 0.076 cm at a cylinder nose. Using Mattas and Smith's curves, if the cooling channel gap were doubled with an attendant increase in coolant pump power, the increase in wall life to double the original swelling would be only about 16%, because most of the wall life is during the gestation period when little swelling occurs. Swelling is also a rapidly increasing function of temperature at the reference design point. Smith and Mattas indicate that raising the temperature from 450 C to 500 C would double the swelling by end of life. Therefore, it appears that any design with steel and high-velocity coolant is limited by excessive swelling limitations to a design life of approximately two years at a neutron wall

loading of 4 MW/m^2 and maximum temperatures of 450 C or higher, independent of whether the reactor plasma is pulsed or unpulsed.

The second most limiting factor in Prevenslik's analysis was brittle fracture, which had a safety margin of 4.3, but was stated to be based on inadequate data on elevated temperature ductility loss in irradiated stainless steel. Using the Fast Breeder Reactor (FBR) Core Components Criteria for predicting brittle fracture, the elastic stress intensity factor K_{max} must be limited to less than two-thirds of the irradiated plane strain fracture toughness K_{IC}. The plane strain fracture toughness decreases under irradiation with the loss in ductility, independent of the number of cycles. For the reference design case, extrapolating from Mattas and Smith's curves, the loss in fracture toughness is roughly a factor of three, corresponding to a tenfold reduction in uniform elongation. The elastic stress intensity factor is a function of the initial crack size and the crack growth rate. Below 425 C, creep-crack growth independent of cycling is negligible. For the reference design case, fatigue-crack growth was 4.5×10^{-10} cm/cycle, corresponding to a total growth of 4.5×10^{-5} cm. The initial crack depth is 0.04 cm, corresponding to the sensitivity of NDT methods of flaw detection. Since the elastic stress intensity factor is proportional to the product of the square root of the crack depth and correction factors based on crack shape, the change in the stress intensity factor due to a 10% change

in the crack length must be negligible. Therefore, even in a steady-state reactor with no crack growth at all, FBR design criteria allow no benefit over the cycled case, because the brittle fracture toughness ratio will decrease as the first wall embrittles. However, since material embrittlement saturates at an asymptotic value of fracture strain, brittle fracture limitations can be overcome for a steady-state reactor, if the asymptotic toughness is greater than 1.5 times the initial stress intensity factor.

The third most limiting factor in Prevenslik's analysis is coolant leakage due directly to excessive crack growth, where 0.1 the original crack length is specified as the highest acceptable crack growth. For the reference design, the safety margin was 89, corresponding to a safety margin of 1 at approximately 10^7 cycles. Since this corresponds to a 20-year life for the reference design, it is not limiting in the neighborhood of this design.

A major consideration when comparing the lifetime of pulsed and unpulsed first walls is that the unpulsed reactor must have a very efficient impurity control method, probably a divertor, and that the pulsed reactor will also require good impurity control. This requirement implies that the charged-particle energy striking the first wall should be small. It now becomes feasible to consider decoupling first-wall cooling from the reactor

thermal cycle. For example, in Prevenslik's report, it was assumed that, with a divertor, the first wall could be operated at a maximum temperature of 270° C., while the maximum blanket temperature would still equal 500° C. By allowing coolant to inlet near the first wall and outlet at the rear of the blanket, it is conceivable that the blanket could be designed so that temperatures are high (∿500° C.) only where neutron irradiation is low. In this case, since the steel is held below the swelling threshold of 350° C., swelling is negligible. Similarly, crack growth in the first wall is neglibible. By assuming the elimination of all bending stress in the first wall cylinders, Prevenslik calculates a safety margin of 12 against brittle fracture. With the obvious caveat that the divertor itself has limitations in handling a high particle heat flux, it appears that neutron wall loading could be significantly increased for either pulsed of steady-state operation. Conversely, neither pulsed nor steady-state first-wall designs would be significantly lifetime limited by operation with a divertor at lower first-wall temperatures and 4 MW/m^2 wall loading. From the above consideration, the possibility emerges that both pulsed and steady-state tokamak reactor first-wall designs will be dictated primarily by their response to off-normal conditions, rather than by fatigue life at normal operating conditions.

Prevenslik[54] and Onega[58] have attempted to make first-order calculations of the effects of plasma disruptions on first-wall lifetime. Both authors state that their work is based on crude assumptions, and neither attaches significant predictive ability to his analyses. The major uncertainties in the analyses include whether disruption-free operating regimes can be identified for ignited plasmas, whether disruptions can be predicted and prevented, whether disruptions will deposit plasma thermal energy evenly over an inner wall surface or whether it will be deposited locally, and whether the direction of motion of plasma disruptions can be infallibly predicted. Onega's study indicated that a 316 stainless-steel first wall would be destroyed due to thermal fatigue after about 450 disruptions, depositing a 185 MJ thermal energy plasma evenly on the inside first wall. Prevenslik concluded that a 10 ms pulse of 75 MW/m^2 would destroy a first-wall module by brittle fracture in a single pulse, before vaporization occurs.

Ignited tokamak plasmas appear to be particularly prone to disruption during the plasma shutdown phase. If plasma current is run-down while the plasma is still at thermonuclear reactor temperatures, large negative skin currents will be formed around an unchanged bulk plasma current, which may be unfavorable for MHD

stability. However, if the plasma is cooled before the current is reduced, it could violate the B_t/R_o limit on plasma density[59] and is predicted to disrupt. Therefore, since fatique life from ordinary nondisruptive operation may not be limiting, there are three alternative comparisons between pulsed and steady-state first-wall designs, depending on experimental results with ignited tokamak plasmas.

(1) If plasma disruptions are a frequent phenomenon, associated with plasma shutdown, only steady-state reactors are viable as a commercial reactor concept.

(2) If plasma disruptions are relatively infrequent, but not completely eliminated, and are unrelated to plasma shutdown, there will be essentially no difference between the designs of steady-state and pulsed first-wall systems.

(3) If plasma disruptions can be totally eliminated, it may be possible to increase first wall lifetime and wall loading, using a steady-state plasma, but it is unclear whether the advantage is really a major one.

6.2.C Poloidal Field System

If the plasma current were started slowly by the application of lower hybrid waves, the voltage requirements of the equilibrium field coils and their power supplies might be greatly reduced. However, as the

recent studies by Bromberg[60] and Schultz[61] imply, the equilibrium field (EF) coil voltage requirements during steady-state burn in a thermally unstable regime could be quite high. For a plasma not in the hot-ion mode, an EF coil requirement comparable to the current-swinging requirement for start-up is needed to hold the plasma radial position against the oscillating radial pressure.[60] However, the rf-driven steady-state current reactor operates in the hot-ion mode, and the ratio of the thermal runaway time to the energy confinement time is much higher, $\tau_{runaway}/\tau_E \simeq 6$, as shown by Bromberg.[62] This thermal runaway time is sufficiently long that particle transport effects may become significant, stablilizing the plasma temperature.

Closely related to the advantages of possible power supply reduction for the equilibrium field coils is the potential of drastically reducing the size of the ohmic heating coils. However, it must be kept in mind that plasma radial controllability requires sufficient power to respond to a perturbation from the desired equilibrium on the order of parameter measurement error in a time on the order of plasma current and temperature decay times in order to avoid frequent plasma-wall collisions. This condition is generally always satisfied by present-day inductive current run-up systems, but it

may be violated by a system which minimizes start-up requirements. An ohmic heating coil or an ECRH delivery system will still be needed for plasma initiation, and some ohmic heating coils may be needed to prevent undesired skin current oscillations, while using the equilibrium field coils to stabilize temperature perturbations.

Ehst[4] has simulated a scenario in which start-up occurs in an EPR-size plasma over a period of 32 seconds, followed by a nine-second main heating phase. If Ehst's scenario can be realized with realistic controllability constraints added, the net flux swing during a cycle will be very small, and the overall cost of the ohmic heating system will be greatly reduced. This will increase the possibility that high electric field induction for initiation from a low-current OH coil will be more desirable than rf-assisted initial breakdown. As Ehst observed, an unsaturated ferromagnetic slug in the machine center will reduce the equilibrium field current requirements by attracting the plasma. It will also reduce ohmic heating coil current requirements by approximately one-half, without a magnetic path return leg.

The trade-off between steady-state current-driven and conventional pulsed tokamak reactors is as follows:

- It is possible that ohmic heating coil current, but not voltage/turn, requirements can be greatly reduced by rf current-driving. There is thus a

real prospect of largely eliminating the cost of the ohmic heating coil and power supply.

- Equilibrium field power supply requirements are determined by controllability for low temperature, thermally unstable operation, whether or not the reactor has steady-state current drive.
- A steady-state current-driven reactor in the hot-ion mode has the potential for significant reduction in active power supply requirements, particularly if disruptions on shutdown are permitted.
- The voltage/turn requirements of both EF and OH coils will probably be dominated by protection against disruptions for all cases.
- The need for a motor-generator-buffer set for the steady-state current-driven reactor is unclear. Some sort of line buffering would probably be needed if several hundred to a few thousand MVA were required for plasma temperature control; but the trade-off between motor-generator-flywheels, reactors, synchronous condensors, and no buffer at all cannot be made at this time.

6.2.D Thermal Storage

An advantage of a steady-state rf current-driven reactor over a pulsed tokamak is that there will be no need for a thermal storage reservoir to permit steam

generation during the dwell time between plasma pulses. As evaluated by Buchanan,[63] a simple increase in the water level of the steam generator, accompanied by a valved pressure reduction during the dwell period, will permit continuous electrical generation at negligible additional cost. This was confirmed for the case of the HFCTR scenario.[5] During the twenty-second dwell time, the boiler steam temperature was permitted to drop to 25° C., while boiler pressure was reduced by 4 MPa.

The HFCTR design conservatively recommended a second thermal reservoir, in order to insure against prolonged outages due to short delays in reestablishing good plasma burn conditions. For concepts requiring secondary heat exchangers, including all blankets cooled by radioactive lithium or lithium salts, a fluidized bed heat exchanger was assessed by Buchanan to add negligible additional cost for thermal storage. The NUWMAK conceptual tokamak reactor [64] recommended the use of the phase transition in a $Li_{62}Pb_{38}$ eutectic blanket to store energy between pulses. If the lithium blanket in HFCTR were replaced by $Li_{62}Pb_{38}$, the enthalpy of phase transition would supply 40 seconds of temperature regulation. If this approach is feasible, it would also reduce thermal cycling in the blanket structure and the rest of the heat transfer and steam generation system. If the incremental costs of two or all of these alternatives are indeed negligible, redundant thermal storage can be provided.

6.2.E Reactor Cost Estimate

It should be emphasized that a quantitative comparison between the costs of steady state and pulsed tokamak reactors cannot be made without much better scenario definition and justification than those available from any previous reactor study and much better knowledge of the disruption histories of the two alternatives. However, for the basis of contrast with the recirculating power and microwave equipment costs of the steady state reactor, a rough comparison between the reference steady-state tokamak reactor specified in Table 1 and the original HFCTR design is made here.

- The short time duty cycle is increased from 85% in the HFCTR pulsed design to 100% in the rf current-driven reactor for a cost savings of 1.18.
- The ohmic heating coil and power supply current ratings are reduced by a factor of ten, for a cost savings of $96.3 M.
- The equilibrium field coil power supply voltage ratings are reduced by a factor of two, for a cost savings of $6.3 M.
- The equivalent power requirements of the motor-generator set are reduced by a factor of two. There is no flywheel. The cost saving is $17 M.
- The ripple coils and their supplies are eliminated for a savings of $6.5 M.

- The recirculating power dissipated by parasitic losses in the poloidal field circuits of HFCTR is 125 MW. This is reduced in the steady-state reactor by 75 MW.
- Because of the reduced ac swinging of the EF coil in the hot ion mode, the electric power for cryogenic refrigeration losses in the TF coils are reduced by 3 MW.
- Electric power for cryogenic losses in neutral beam cryopanels is reduced by 2.0 MW.
- Electric power for cryogenic losses in the OH and dipole coils is reduced by 2.0 MW.
- The corresponding decrease in the cost of the cryogenic refrigeration system is $2 M.
- The averaged power for the neutral beam power supply system of 4.4 MW is eliminated.
- The ripple coil losses of 1.0 MW are eliminated.
- The cost of the neutral beam system in HFCTR is listed as $100 M, but this should be $140 M.
- Plant availability is arbitrarily assumed to increase by 10% by virtue of the fatigue-free steady-state operation.
- Building costs of electrical plant structure and reactor support structure are reduced by $7.5 M, with the replacement of the neutral beam system by lower hybrid.

Therefore, before adding the cost and recirculating power of the lower hybrid rf system, the cost of the HFCTR reactor has decreased from $1,263.0 M to $987 M. The available

net electrical output has increased from 648 to 892 MW, or 1,027 MW gross minus 135 MW recirculating, instead of 870 MW gross minus 22 MW recirculating. Plant availability increased from 70 to 77%. Thus, even without predicting dramatic improvements in reactor economies due to first wall life, an upper bound on the improvement in HFCTR economies is a factor of 1.9, if the cost of current driving were negligible.

For the reference case, with a Q of 40, the steady-state power into the plasma is 61.5 MW. Assuming that a Q = 25 or 100 MW rf system is needed to heat the plasma to ignition, the cost of the rf microwave equipment is $75 M, as shown in Table 4. With the assumption of 80% efficient coupling into the plasma with direct energy recovery, the recirculating losses are 91 MW, as calculated in section 6.2. The net electrical output is then 801 MW at a building and equipment cost of $1,062 M. Therefore, the improvement in reactor economics over the HFCTR, predicted by the above-mentioned models and assumptions, is a factor of 1.6. With the given models, the cross-over value of Q for the current-drive at which the overall economics of the steady-state reactor would equal those of the original HFCTR is Q = 11. We repeat the caveats that both designs are probably inconsistent because of the lack of a divertor and that the physics uncertainty associated with this comparison is extremely high. It should also be noted that the economies of the present

reference design over the HFCTR are caused by the combination of steady-state operation, operation in the hot-ion mode and replacement of neutral beams by microwave heating, and are not a function of steady-state operation alone. Nevertheless, we believe that the above analysis supports the following encouraging conclusions:

- The steady-state current driven reactor concept has the potential for making the cost reductions of a factor of about two, believed to be necessary to allow commercial fusion reactors to compete directly with conventional sources of electricity, such as coal or nuclear power.
- The recirculating power requirements of a high-Q driven reactor are not necessarily higher than the recirculating power for a pulsed, ignited reactor, when burn control power is taken into account.

ACKNOWLEDGMENT

We would like to thank L. Bromberg, D. A. Ehst, J. Fischer, D. F. F. Karney, J. Kulp, and J. J. Schuss for helpful discussions.

REFERENCES

[1] N.J. Fisch and A. Bers, in Proc. of the Third Topical Conference on RF Plasma Heating, Pasadena, 1978.

[2] N.J. Fisch, Phys. Rev. Letters 41, (1978), 873.

[3] R. Prater, et al., General Atomic Company Report GA-A15229, (1978); GA-A15385, (1979).

[4] D.A. Ehst, Argonne National Laboratory, ANL/FPP/TM-120, (1979), (to be published in Nuclear Fusion).

[5] D.R. Cohn, et al., M.I.T. Plasma Fusion Center Research Report RR-78-2 and RR-79-2.

[6] L. Bromberg, D.R. Cohn, and J. Fischer, M.I.T. Plasma Fusion Center Report RR-79-3 (to be published in Nuclear Fusion).

[7] A.A. Vedenov, in Review of Plasma Physics, (Consultant Bureau, New York, 1967), Vol. 3.

[8] C.F.F. Karney and N.J. Fisch, Princeton Plasma Physics Laboratory Report PPPL-1506, (1979), (to be published in Phys. Fluids).

[9] K.L. Wong, Phys. Rev. Letters 43, (1979), 438.

[10] R.J. La Haye, et al., General Atomic Company Report GA-A15376, (1979).

[11] S.C. Luckhardt, Bull. Am. Phys. Soc., (1979).

[12] D.A. Ehst, private communication.

[13] W.H. Hooke, private communication.

[14] M. Brambilla, Nuclear Fusion 16, (1976), 47.

[15] S. Bernabei and I. Fidone, Third Sym. on Plasma Heating in Tor. Dev., Varenna, (1976), Editrice Compositori, Bologna, Italy, 1976), 92.

[16] V. Krapchev and A. Bers, Nuclear Fusion 18, (1978), 519.

[17] S. Bernabei, et al., Nuclear Fusion 17, (1977), 929.

[18] S. Bernabei, et al., Third Sym. on Plasma Heating in Tor. Device, Varenna, (1976), 68.

[19] J.J. Schuss, et al., Phys. Rev. Letters 43, (1979), 274.

[20] T. Nagashima, et al., Int. Sym. on Heating in Toroidal Plasma, Grenoble, France, (1978), (Permagon, N.Y., 1979), Vol. 2, 281.

[21] T. Imai, et al., Phys. Rev. Letters 43, (1979), 586.

[22] R.J. Briggs and R.R. Parker, Phys. Rev. Letters 29, (1972), 852

[23] P.M. Bellan and M. Porkolab, Phys. Fluids 17, (1974), 1,592.

[24] P.M. Bellan and M. Porkolab, Phys. Rev. Letters 34, (1975), 124.

[25] S. Takamura, et al., Nuclear Fusion (to be published).

[26] P.P. Lallia, et al., Third Sym. on Plasma Heating in Toroidal Device, Varenna, (1976), 79.

[27] R.L. Freeman, et. al., Proc. 7th Int. Conf. Controlled Nuclear Fusion Research, Vienna, (1979), Vol. 1, 157.

[28] V.M. Glagolev, Plasma Phys. 14, (1972), 301.

[29] V.E. Golant, Soviet Phys. Tech. Phys. 16, (1972), 1,980.

[30] T.H. Stix, Phys Rev. Letters 15, (1965), 878.

[31] M. Porkolab, Phys. Fluids 20, (1977), 2,058.

[32] M. Porkolab, et al., Phys. Rev. Letters 38, (1977), 230.

[33] J. Kulp, Ph.D. Thesis, Dept. of Elec. Eng., M.I.T., (1978).

[34] M. Porkolab and R.P.H. Chang, Rev. Mod. Phys. 50, (1978), 745.

[35] R.E. Slusher and C.M. Surko, Phys. Rev. Letters 40, (1978), 400.

[36] P.M. Bellan and K.L. Wong, Phys. Fluids 21, (1978), 592.

[37] V.B. Krapchev and A.K. Ram, M.I.T. RLE Plasma Research Dept. PRR 79114.

[38] M. Porkolab, Nuclear Fusion 18, (1978), 367.

[39] K.L. Wong, P. Bellan, and M. Porkolab, Phys. Rev. Letters 40, (1978), 554.

[40] M. Porkolab, Phys. Fluids 17, (1974), 1,432.

[41] D.R. Cohn, R.R. Parker, D.L. Jassby, Nucl. Fusion 16, (1976), 31; D.L. Jassby, D.R. Cohn, R.R. Parker, Nucl. Fusion 16, (1976), 1,045.

[42] D.G. McAlees, Oak Ridge National Laboratory Report ORNL-TM-4661, (1974).

[43] D.L. Jassby, in Plasma Heating in Toroidal Devices, Varenna, Italy, (1974), 259.

[44] T.H. Stix, Plasma Phys. 14, (1972), 367.

[45] K. Molvig, private communication.

[46] B.W. Reed, "Preliminary Report on the Development of RF Auxiliary Heating Systems for TEPR-1," Princeton Plasma Physics Laboratory, PPPL-1410, Dec. 1977.

[47] J.F. Skowron, W.C. Brown, and G.H. MacMaster, "The Super Power CW Amplitron," Microwave Journal, Oct. 1964.

[48] A. Goldfinger, "High Power RF Window Study," Technical Report No. RADC-TR-66-657, Jan. 1967.

[49] F.O. Johnson, "Waveguide Windows for Multi-Kilowatt Applications," Proc. of Internat'l. Conf. on Microwave Circuit Theory and Information Theory, Tokyo, Japan, Sept. 7-11, 1964.

[50] K. Rice, private communication; Model CCH 95 circulator, Final Acceptance Record.

[51] Westinghouse Electric Corporation, Electrical Transmission and Distribution Reference Book, 1964.

[52] W. C. Brown, "Microwave Energy Transmission," Third Princeton/AIAA Conference on Space Manufacturing Facilities, Princeton, N.J., May, 1977.

[53] J.F. Skowron, "The Continuous-Cathode (Emitting-Sole) Crossed-Field Amplifier," Proc. of the IEEE, Vol. 61, No. 3, March 1973.

[54] T.V. Prevenslik, "Structural Evaluation of a Tokamak Reactor Cylindrical Module Blanket Concept," Westinghouse Fusion Power Systems Dept., WFPS-TME-096, Oct. 1978.

[55] R.F. Mattas and D.L. Smith, "Model for Life--Limiting Properties of Fusion Reactor Sturctural Materials," Nucl. Tech., Vol. 39, Jy. 1978.

[56] J.S. Karbowski et al., "Tokamak Blanket Design Program: Final Report," Westinghouse Fusion Power Systems Dept., NFPS-TME-102, Oct. 1978.

[57] J.E. Meyer, "Structural Advantages of Steady State Fusion Power Reactors: MIT Plasma Fusion Center Report PFC/TR-78-3, Mar. 1978.

[58] R.J. Onega, W.R. Becraft, E.A. Bettis, "Major Plasma Disruptions in TNS," Oak Ridge National Laboratory, ORNL/TM - 6616, Feb. 1979.

[59] M. Murakami et al., Nucl. Fusion 16, (1976), 347.

[60] L. Bromberg, J.L. Fisher and D.R. Cohn, Nucl. Fusion 19 (1979) 1359.

[61] J.H. Schultz, L. Bromberg and D.R. Cohn, "Ignition and Thermal Stability Characteristics of Advanced Fuel Plasmas," M.I.T. Plasma Fusion Center Report RR-79-5, July, 1979.

[62] L. Bromberg, D.R. Cohn, J. Fisher, "Regimes of Ignited Operation," M.I.T. Plasma Fusion Center Report RR-79-3, March 1979.

[63] C.H. Buchanan, "Energy Storage for Tokamak Reactor Cycles," Princeton Plasma Physics Laboratory, PPL-1511, Jan. 1979.

[64] R.W. Conn, G.L. Kulcinski, C.W. Maynard, "NUWMAK: An Attractive Medium Field, Medium Size, Conceptual Tokamak Reactor," University of Wisconsin Report UWFDM-249, May 1978.

Table 1

REFERENCE PARAMETERS FOR A REACTOR WITH Q = 40 AND PARABOLIC CURRENT PROFILE

Machine Parameters:	
major radius R	6.0 m
plasma halfwidth a	1.2 m
aspect ratio A	5.0
plasma shape factor S	1.5
field at plasma B_o	7.4 T
field at coil B_{To}	13.1 T
plasma volume V_p	317
first wall area A_W	475
Plasma Parameters:	
safety factor q(a)	3.4
average toroidal beta $\bar{\beta}_t$	.038
plasma current I_p	5.3 MA
electron density n_e	$2.0 \times 10^{20}(1-\rho^3)m^{-3}$
electron temperature T_e	$23(1 - \rho^2)$ KeV
ion temperature T_i	$34(1 - \rho^2)$ KeV
Z_{eff}	1
Microwave System:	
frequency f	2.79 GHz
spectral location n_z	1.5 - 1.6
total wave power P_{rf}	72 MW
total waveguide area A_G	14.5 m
average wave power flux S	5 MW/m^2
Power Production:	
total fusion power $\bar{P}_f V_p$	2900 MW
average fusion power density $\bar{P}_f$	9.1 MW/m^3
plasma Q	40
duty cycle	100%
neutron wall loading	4.7 MW/m^2
average thermal power P_{th}	2930 MW
gross electric power (35% eff.)	1027 MW
recycled electric power as microwave	91 MW
other recycled electric power	135 MW
net electric power	800 MW

m_n	m_t	m_j	Q
.8	.8	.8	38
.8	.8	1	37
.8	1	1	36
2	.8	1	36
1	1	1	35
1	1	2	33
1	2	1	33
2	2	2	28

TABLE 2

Effect of plasma profiles on $Q = P_F/\bar{P}_D$.

$n = n_o(1 - \rho^2)^{m_n}$, $T = T_o(1 - \rho^2)^{m_t}$, $J = J_o(1 - \rho^2)^{m_j}$,

$R = 6$ m, $A = 5$, $B_o = 7.5$, $S = 1$, $\bar{T}_e = 15$ KeV,

$\bar{T}_i = 22$ KeV, $\bar{n}_{20} = \bar{n}_{ign} = 0.57$.

Table 3

Microwave Component Ratings for Lower Hybrid Steady-State Current Driven Tokamak Reactor

High-voltage rectifier	144 MW
Regulated high-voltage d.c. supplies	133 MW
Power Crossed-Field Amplifiers	135 MW
Input Amplifiers	3.4 MW
Circulators	156 MW
Waveguide	156 MW
Windows	148 MW

Table 4

Cost of Microwave Power Delivery System for Bulk Heating and Current Driving of Steady-State Tokamak Reactor

High-voltage regulated d.c. supply, including rectifier and rectifier-transformer	$17.0 M
Output Stage Crossed-Field Amplifiers	38.2 M
Driver Amplifiers	1.2 M
Circulators	1.7 M
Waveguide	7.8 M
Windows	5.0 M
Miscellaneous Microwave Components	3.8 M
TOTAL	$74.7 M

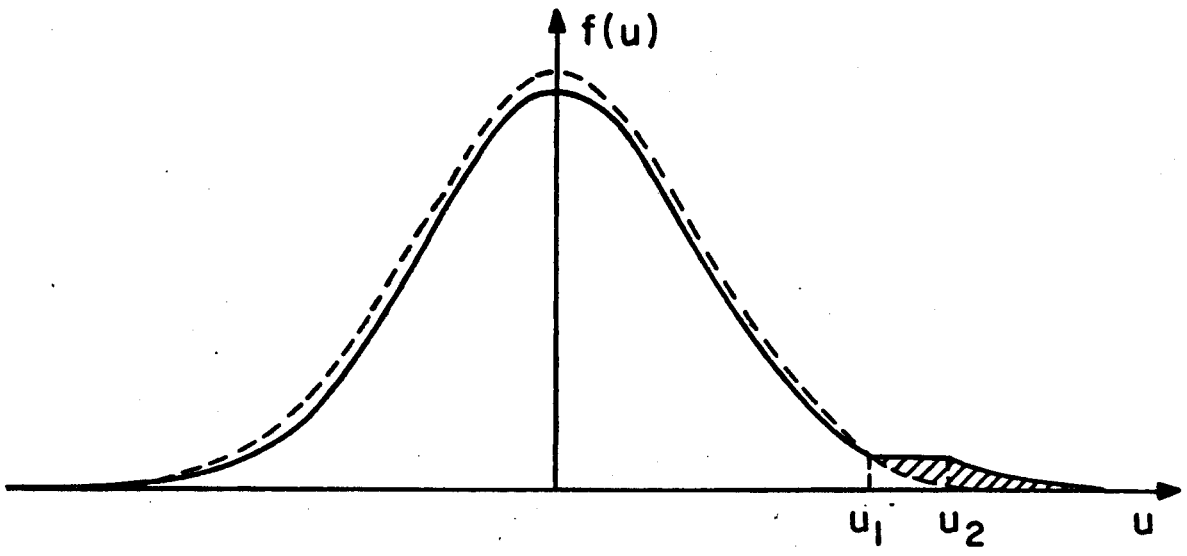

FIG. 1. Schematic diagram for the parallel electron distribution function. The dashed line gives the undisturbed Maxwellian distribution. The solid line gives the distribution function in the presence of rf wave with phase velocity $u_1 \leq u \leq u_2$. Current is carried by electrons in the shaded portion.

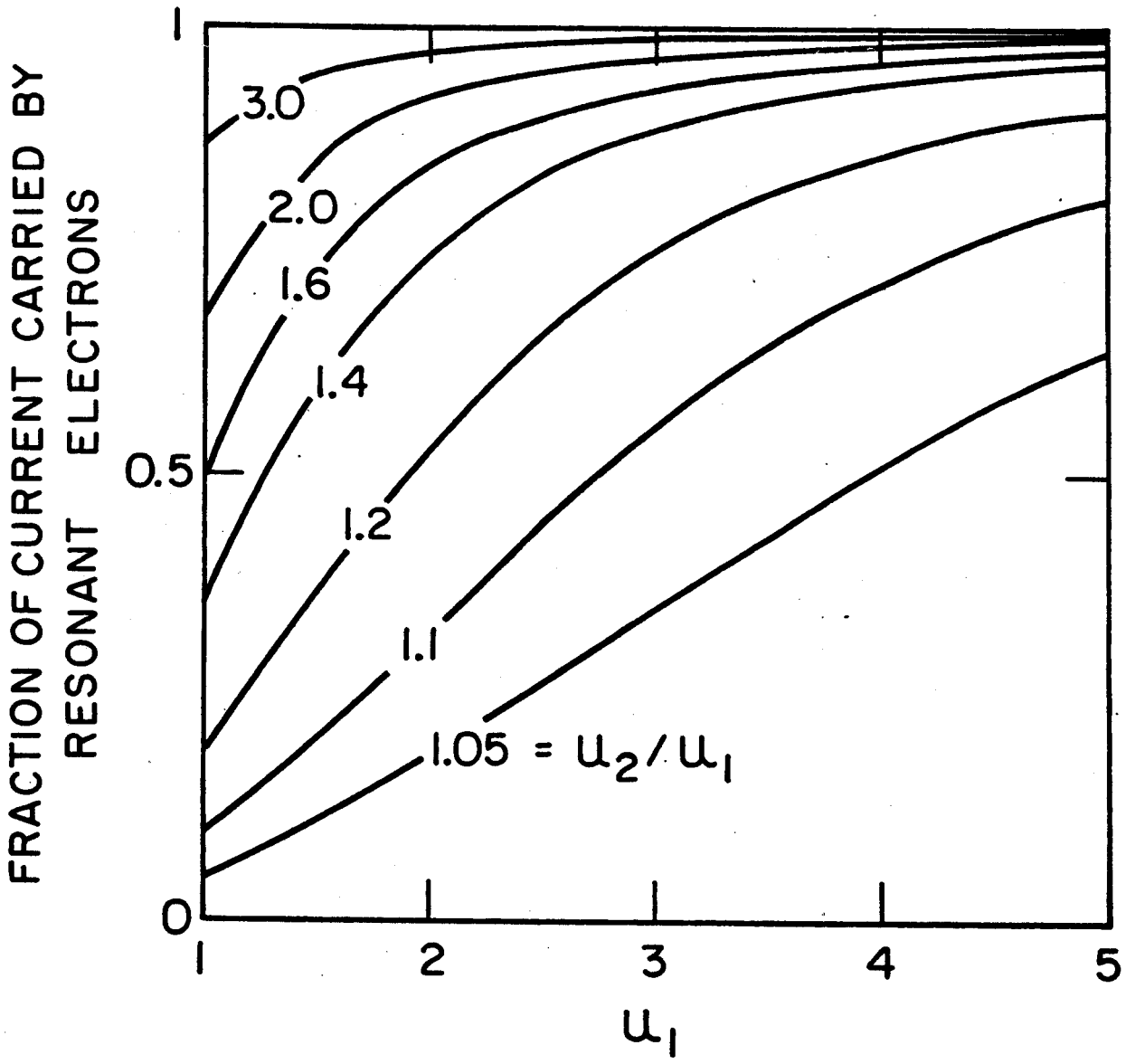

FIG. 2. Fraction of rf generated current carried by resonant electrons.

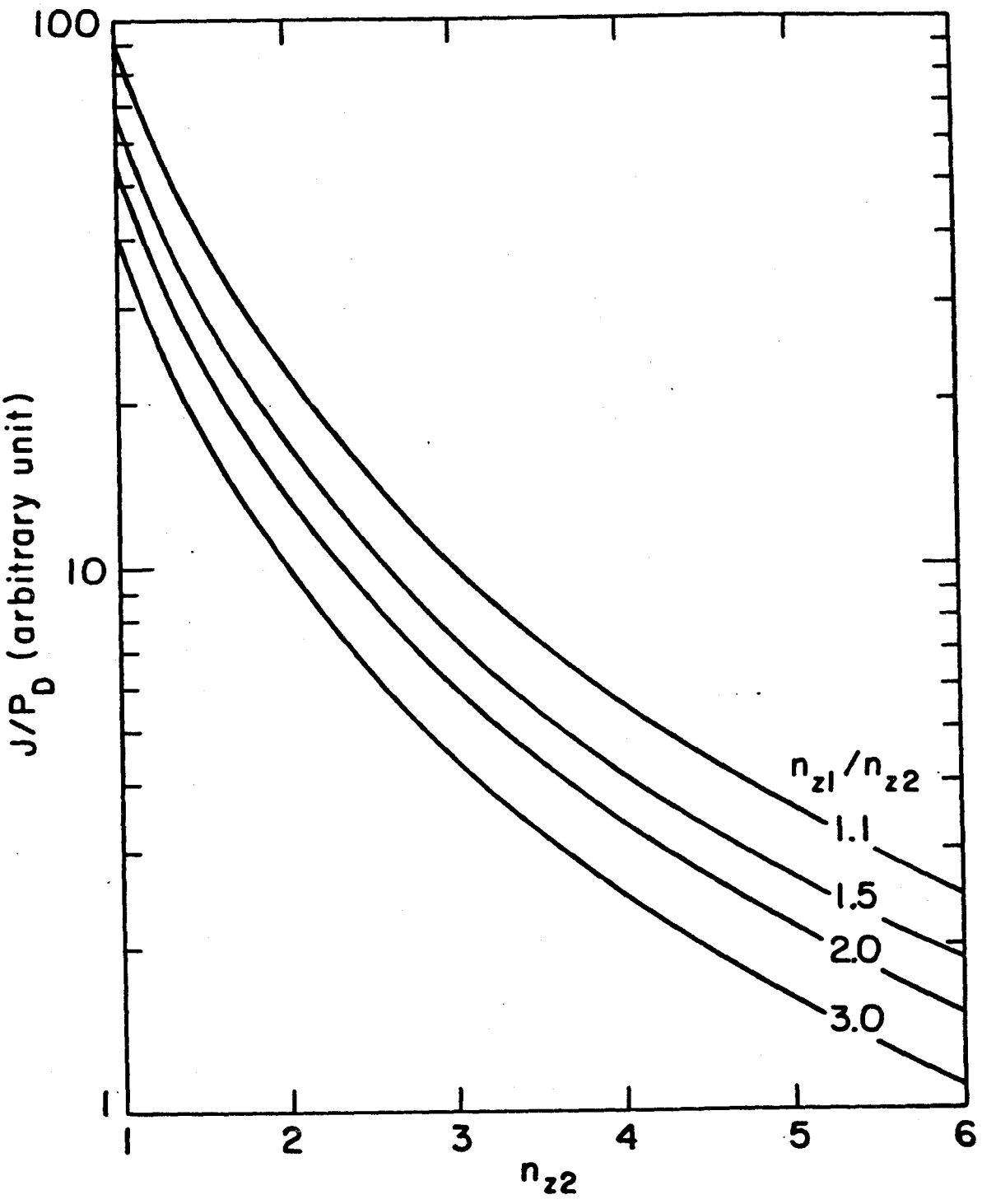

FIG. 3. Effectiveness of rf current generation as a function of the parallel refractive index of the lower hybrid wave.

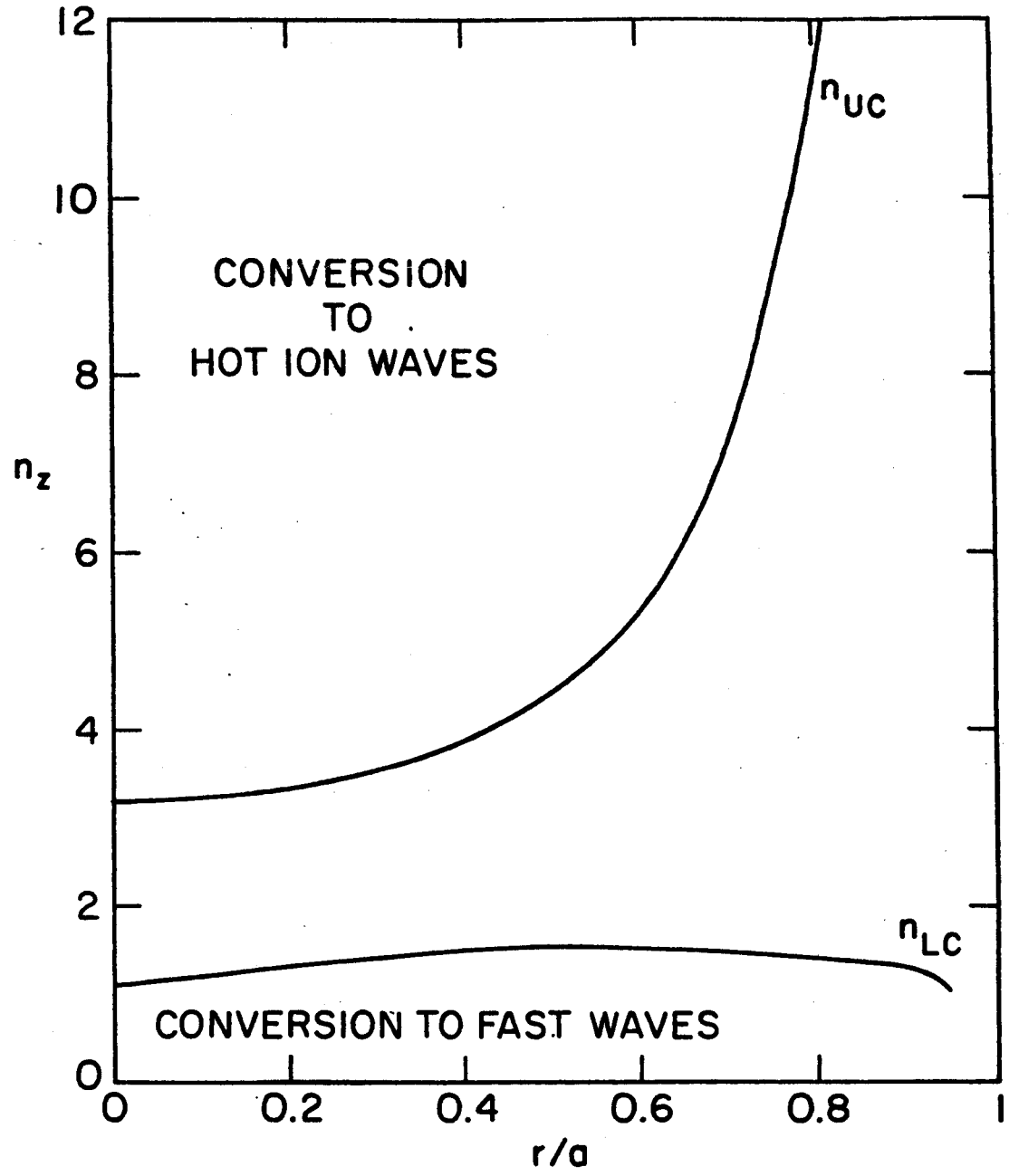

FIG. 4. Radial profile of accessibility condition (n_{LC}) and mode conversion layer (n_{UC}). Slow wave with $n_{LC} < n_z < n_{UC}$ can propagate. [$\bar{T}_e$ = 15 KeV, B_o = 7.5 T, $\bar{n}_e = 10^{20} m^{-3}$, $\omega = 2\omega_{LH}(0)$].

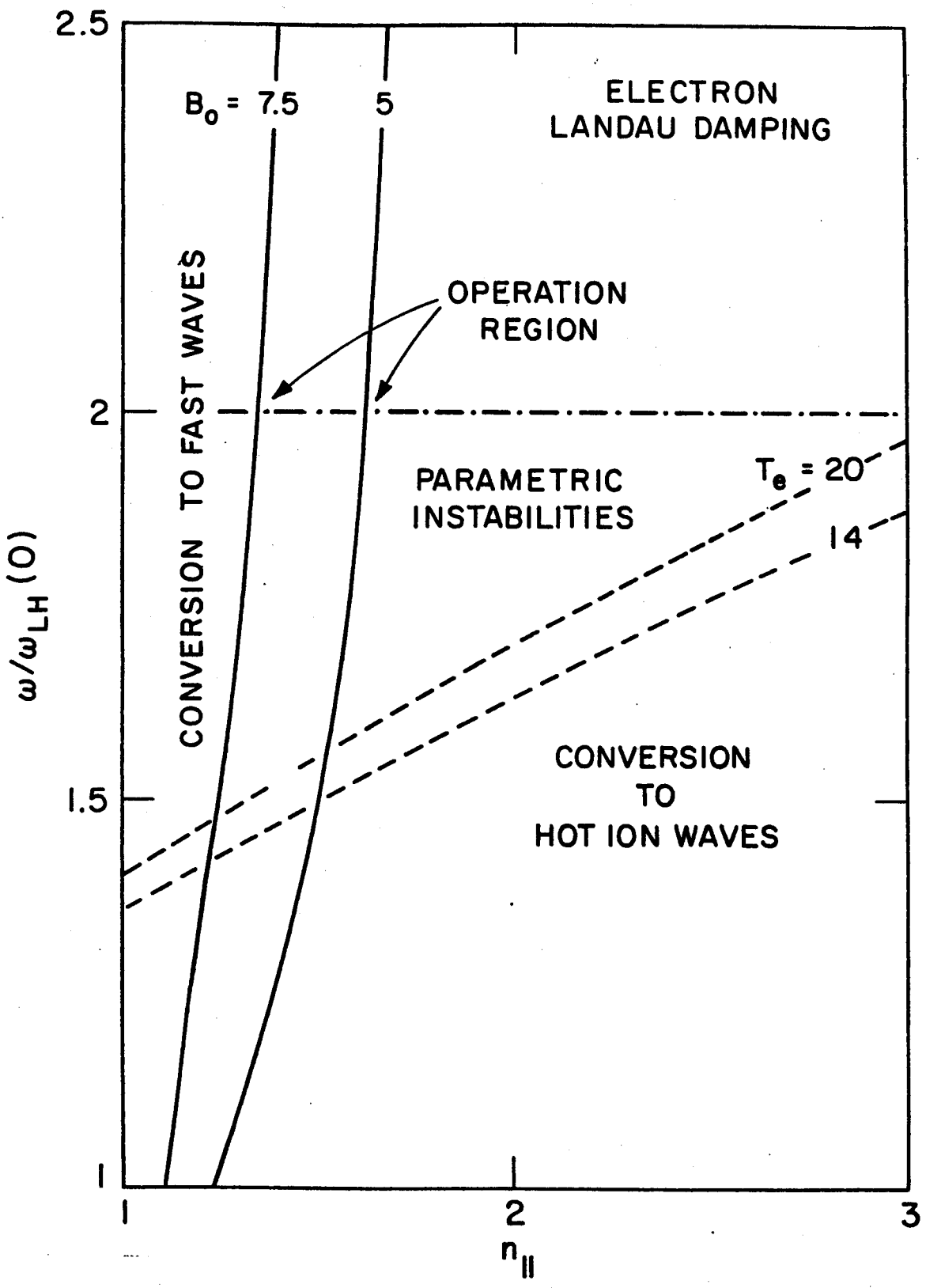

FIG. 5. Regions of wave-plasma interaction in the parameter space of lower hybrid wave. The solid lines are n_{LC} for $\bar{T}_e$ = 14 KeV and B_o = 7.5, 5T. The dashed lines are n_{UC} for B_o = 7.5 T and $\bar{T}_e$ = 14, 20 KeV [$\bar{n}_e = 10^{20} m^{-3}$].

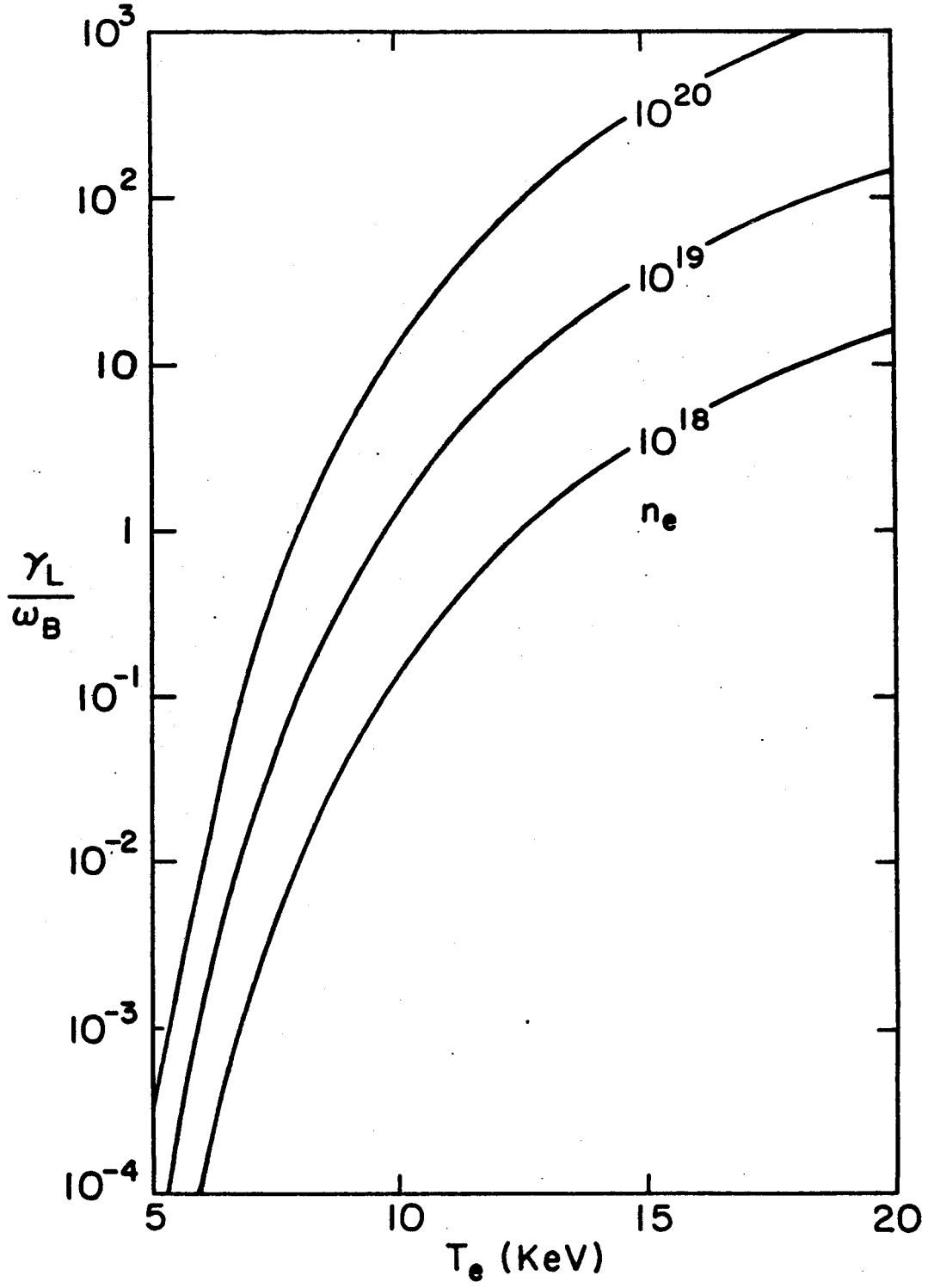

FIG. 6. Trapping parameter as a function of electron temperature. Trapping will occur if $\gamma_L/\omega_B < 1$.

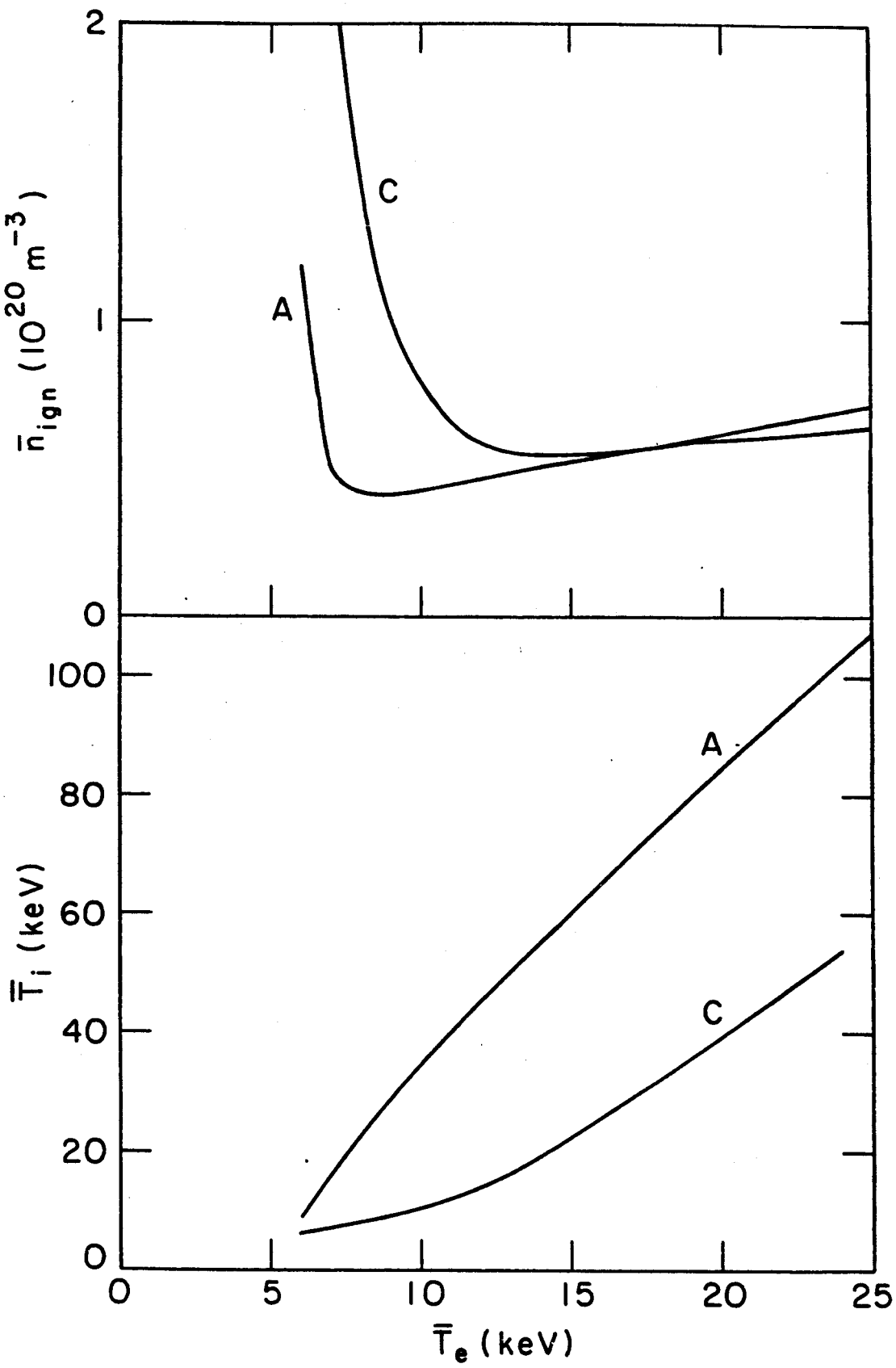

FIG. 7. Averaged ion temperature (solid curves) and $\bar{n}_{ign}$ (dashed curves) as a function of $\bar{T}_e$. Curves marked (A) are for classical alpha slowing down and (C) for anomalous alpha-slowing-down. [R = 6m, A = 5, B_o = 7.5 T, S = 1].

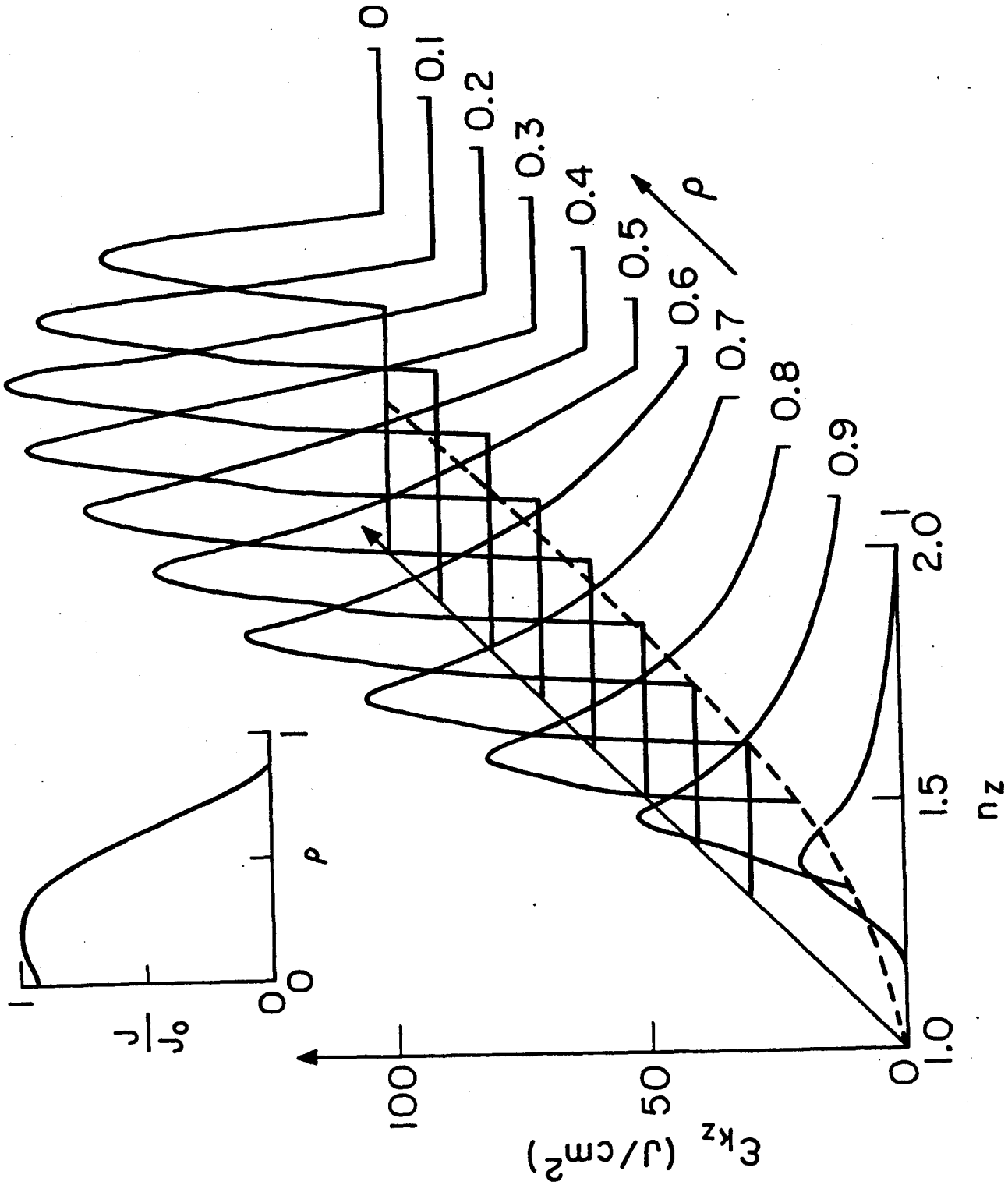

FIG. 8. Variation of the slow wave spectrum as it propagates from the plasma edge ($\rho = 1$) to the center ($\rho = 0$). The dashed curve shows n_{LC}. The rf-driven current profile is depicted in the insert. [R = 6 m, A = 5, B_o = 7.5 T, S = 1, $\bar{T}_e$ = 14 KeV, $\bar{T}_i$ = 19 KeV, $\bar{n}_{20}$ = 0.59, $n_e = n_{eo}(1-\rho^3)$, $T = T_o(1 - \rho^2)$, f = 2.21 GHz, I_p = 2.4 MA, $Q = P_F/P_D$ = 33].

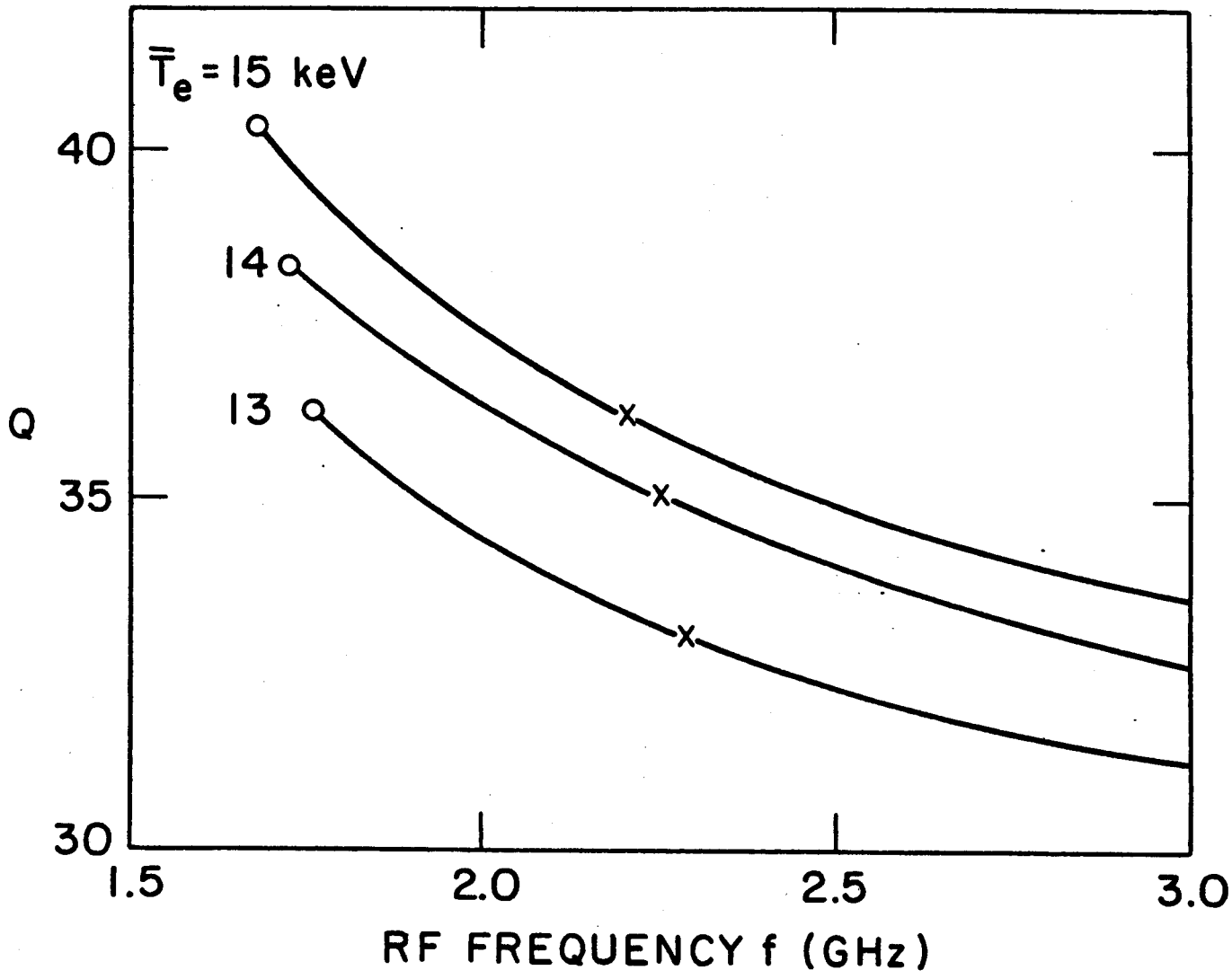

FIG. 9. Fusion to rf power ratio as a function of rf frequency for several electron temperatures. The circle marks for each case $\omega = \omega_{min}$ and the cross marks $\omega = 2\omega_{LH}(0)$. [R = 6 m, A = 5, B_o=7.5T, S = 1, $\bar{T}_e$ = 15 KeV, $\bar{T}_i$ = 22 KeV, $n = n_{eo}(1 - \rho^3)$, $T = T_o(1 - \rho^2)$, $J = J_o(1 - \rho^2)$, $\bar{n} = \bar{n}_{ign}$].

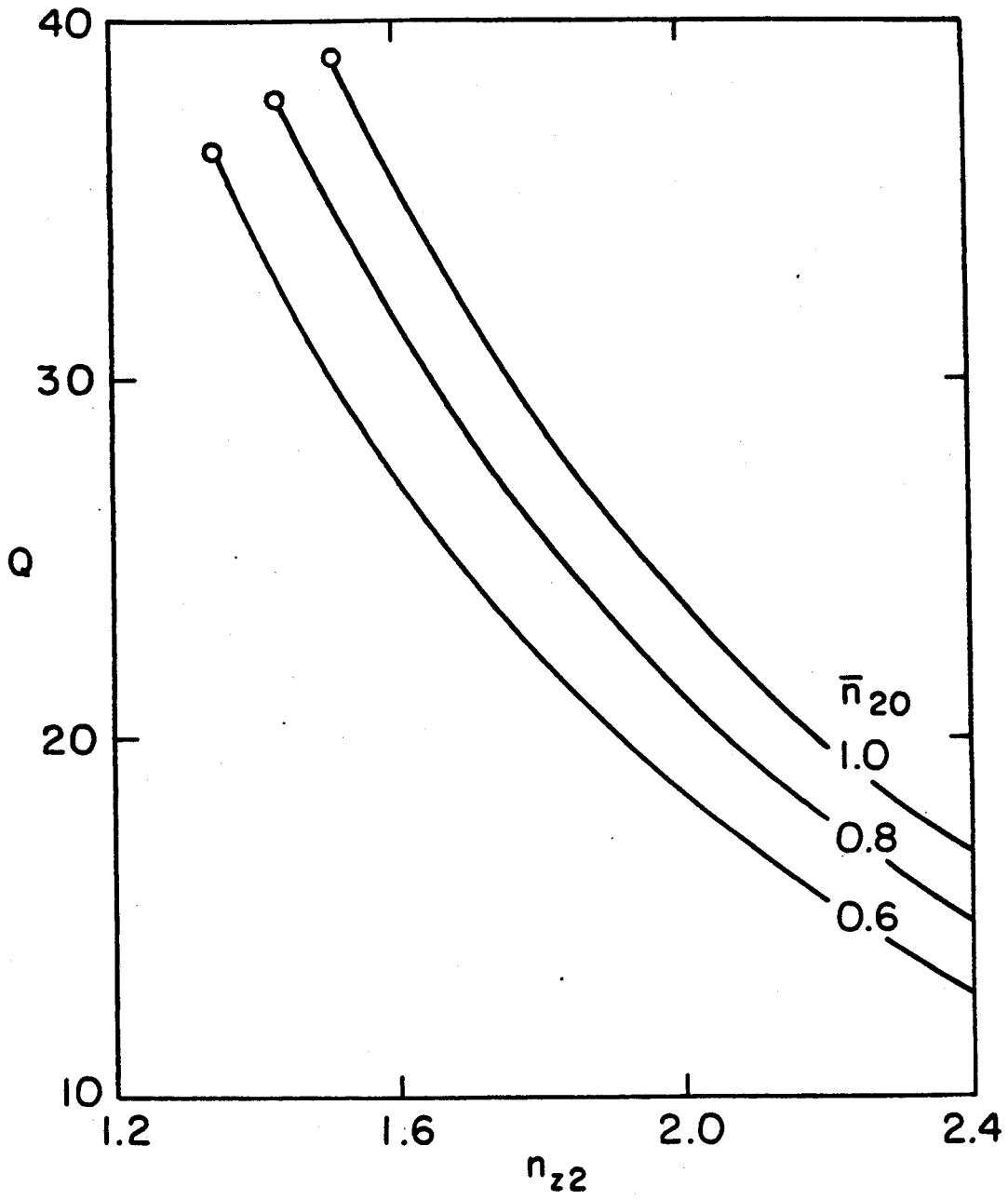

FIG. 10. Fusion to rf power ratio as a function of parallel index of refraction. The circles mark the minimum n_z allowed by accessibility condition. [R = 6 m, A = 5, B_o = 7.5 T, S = 1, $\bar{T}_e$ = 15 KeV, $n=n_{eo}(1-\rho^3)$, $T = T_o(1 - \rho^2)$, $J = J_o(1 - \rho^2)$].

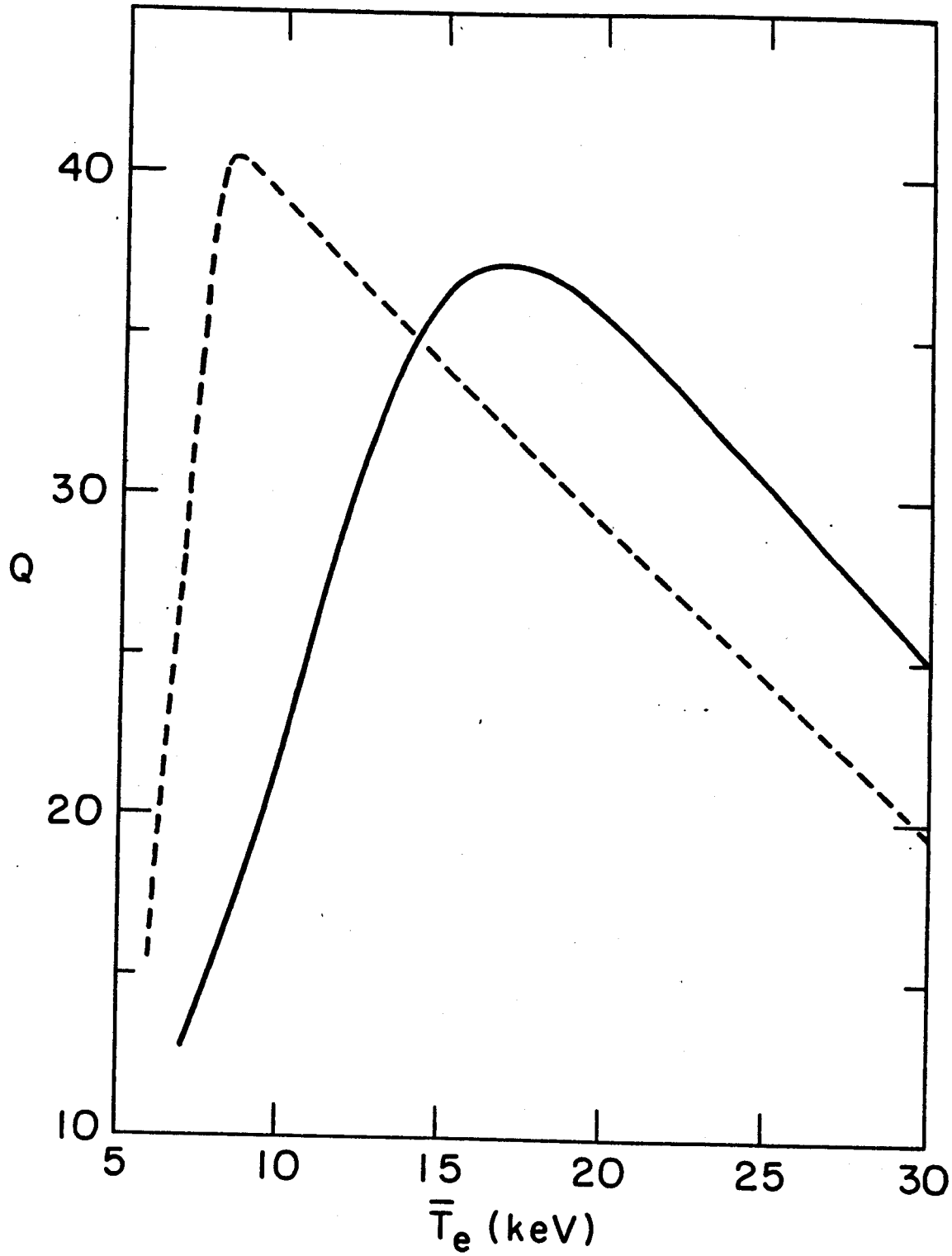

FIG. 11. Fusion to rf power ratio versus $\bar{T}_e$. Solid curves: classical alpha-slowing-down; dashed curves: anomalous alpha-slowing-down. [R = 6 m, A = 5, B_o = 7.5 T, S = 1, $\bar{n}_e = \bar{n}_{ign}$, $n_e = n_{eo}(1-\rho^3)$, $T = T_o(1-\rho^2)$, $J = J_o(1-\rho^2)$, $\omega = 2\omega_{LH}(0)$].

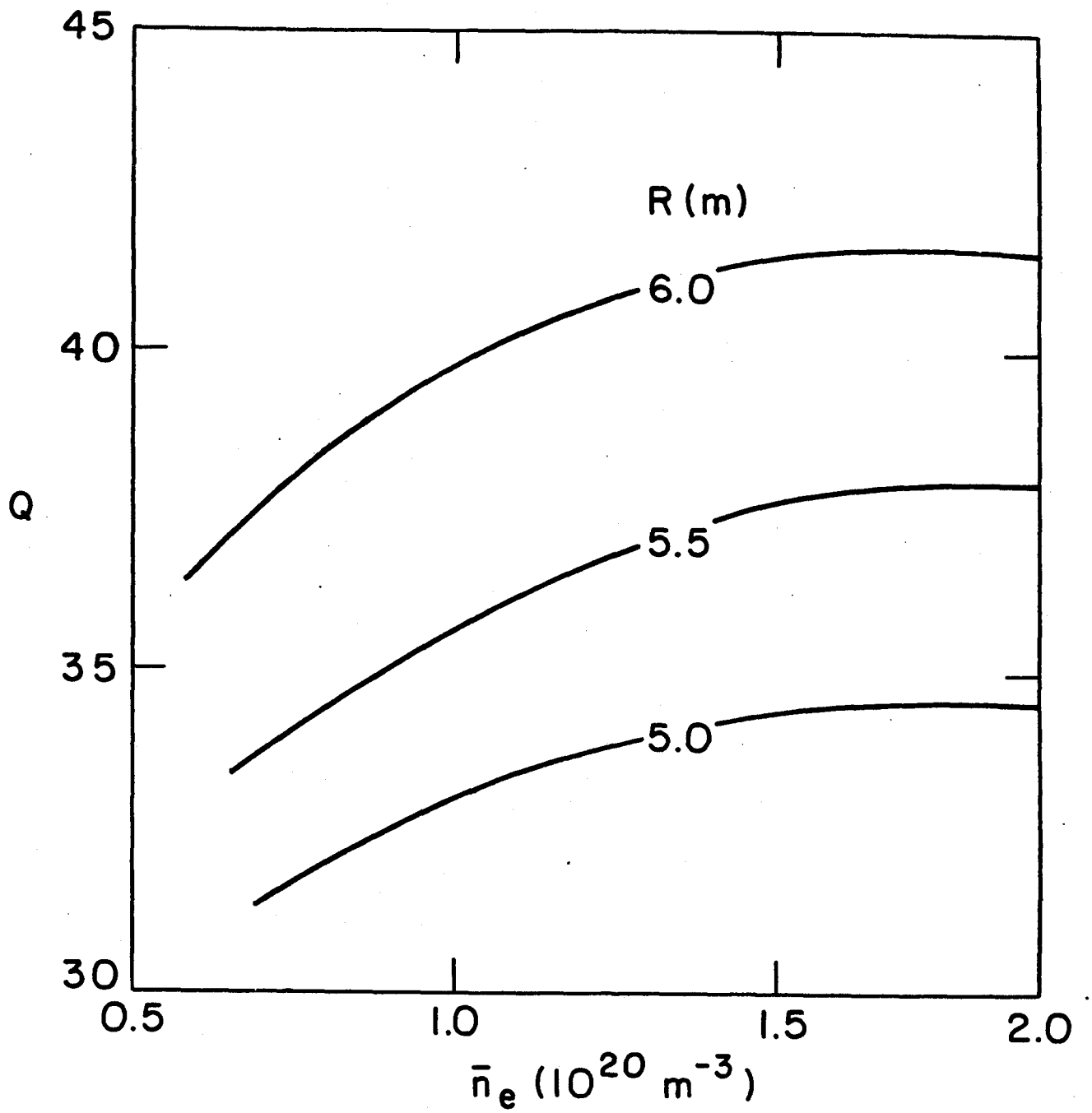

FIG. 12. Dependence of Q on averaged plasma density [R = 6 m, A = 5, B_o = 7.5 T, S = 1, $\bar{T}_e$ = 15 KeV, $\bar{T}_i$ = 22 KeV, $n_e = n_{eo}(1 - \rho^3)$, $T = T_o(1 - \rho^2)$, $J = J_o(1 - \rho^2)$, $\omega = 2\omega_{LH}(0)$].

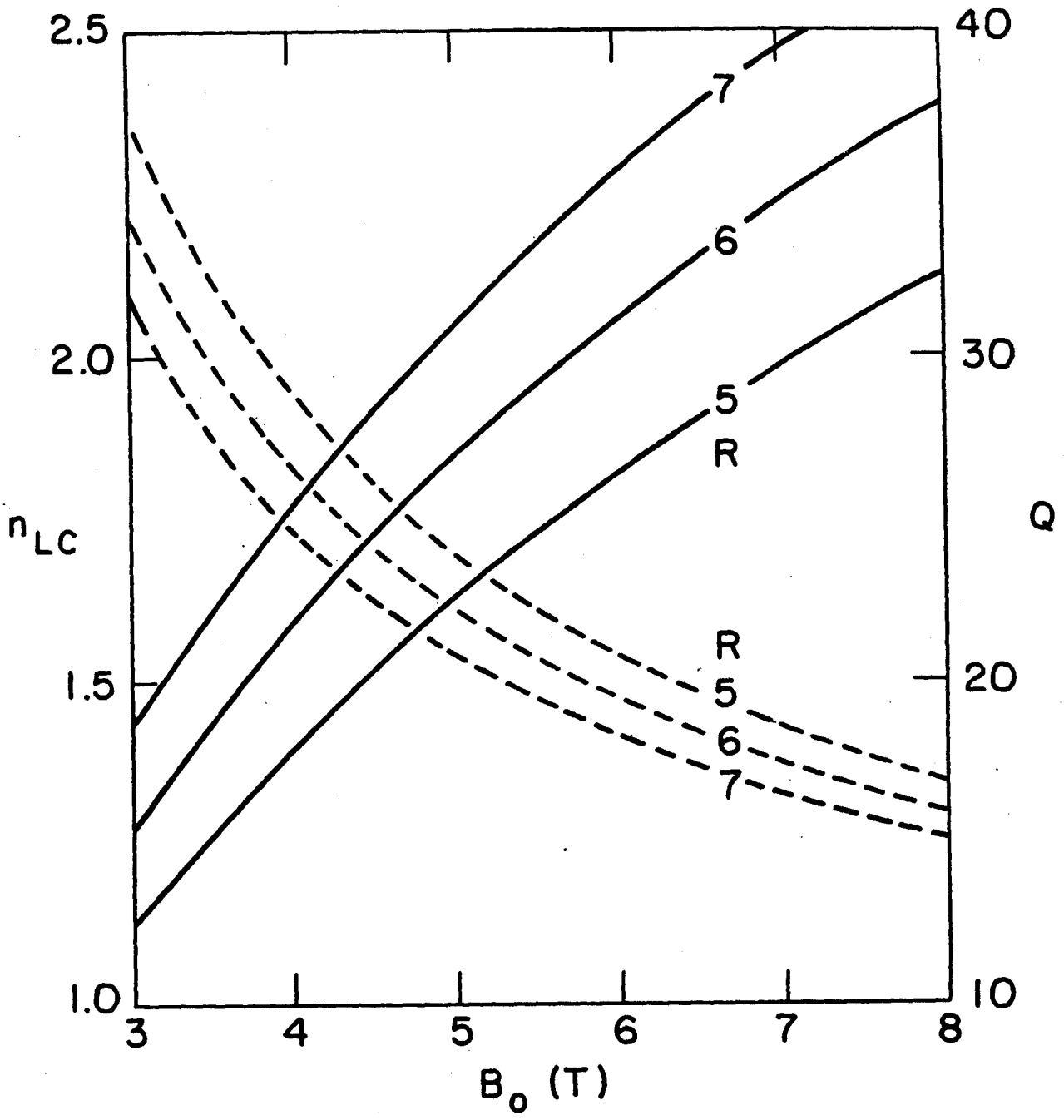

FIG. 13. Accessibility condition of the lower hybrid wave, n_{LC}, as a function of magnetic field (dashed curves). The solid curves give the corresponding fusion to rf power ratio for several size reactors. [A = 5, S = 1, $n_e = n_{eo}(1-\rho^3)$, $T = T_o(1-\rho^2)$, $J = J_o(1-\rho^2)$, $\bar{T}_e$ = 15 KeV, $\bar{T}_i$ = 22 KeV, $\bar{n}_{20}$ = 0.57, $\omega = 2\omega_{LH}(0)$].

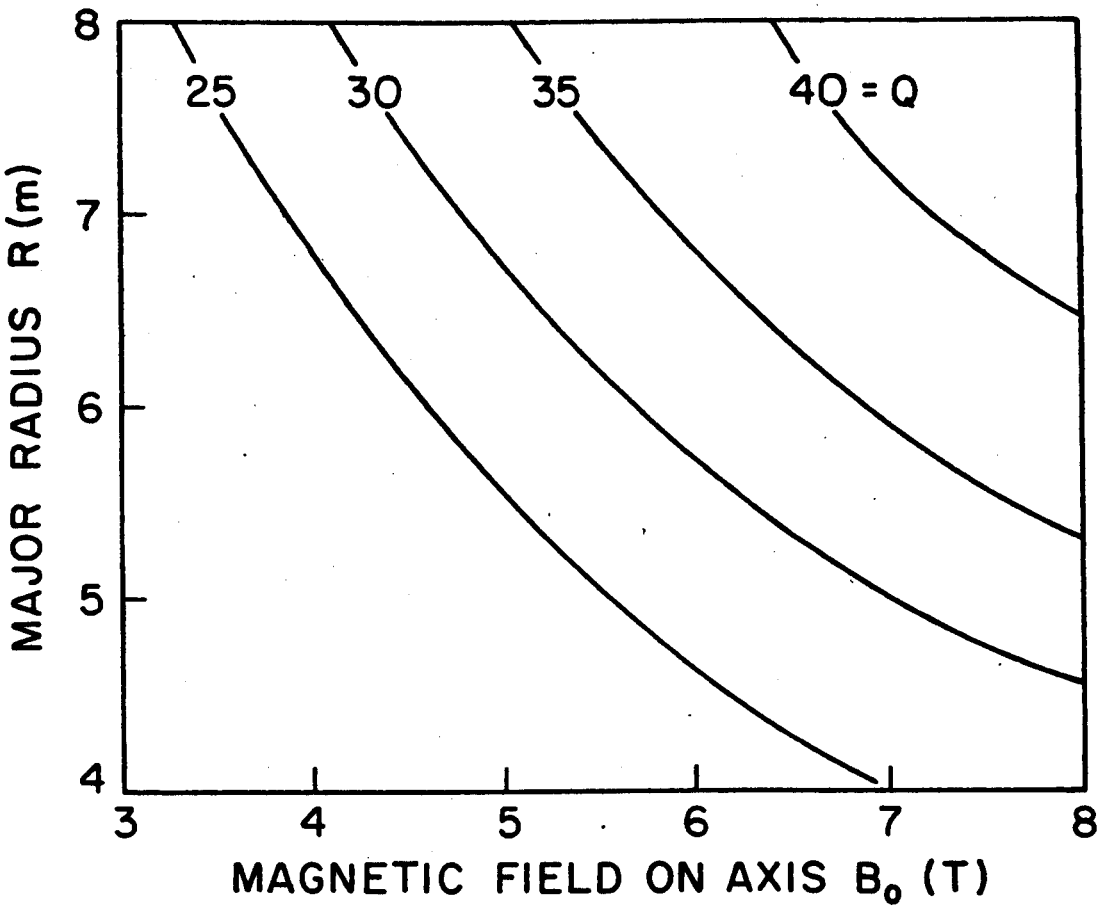

FIG. 14. Trade off between reactor size and toroidal magnetic field strength.

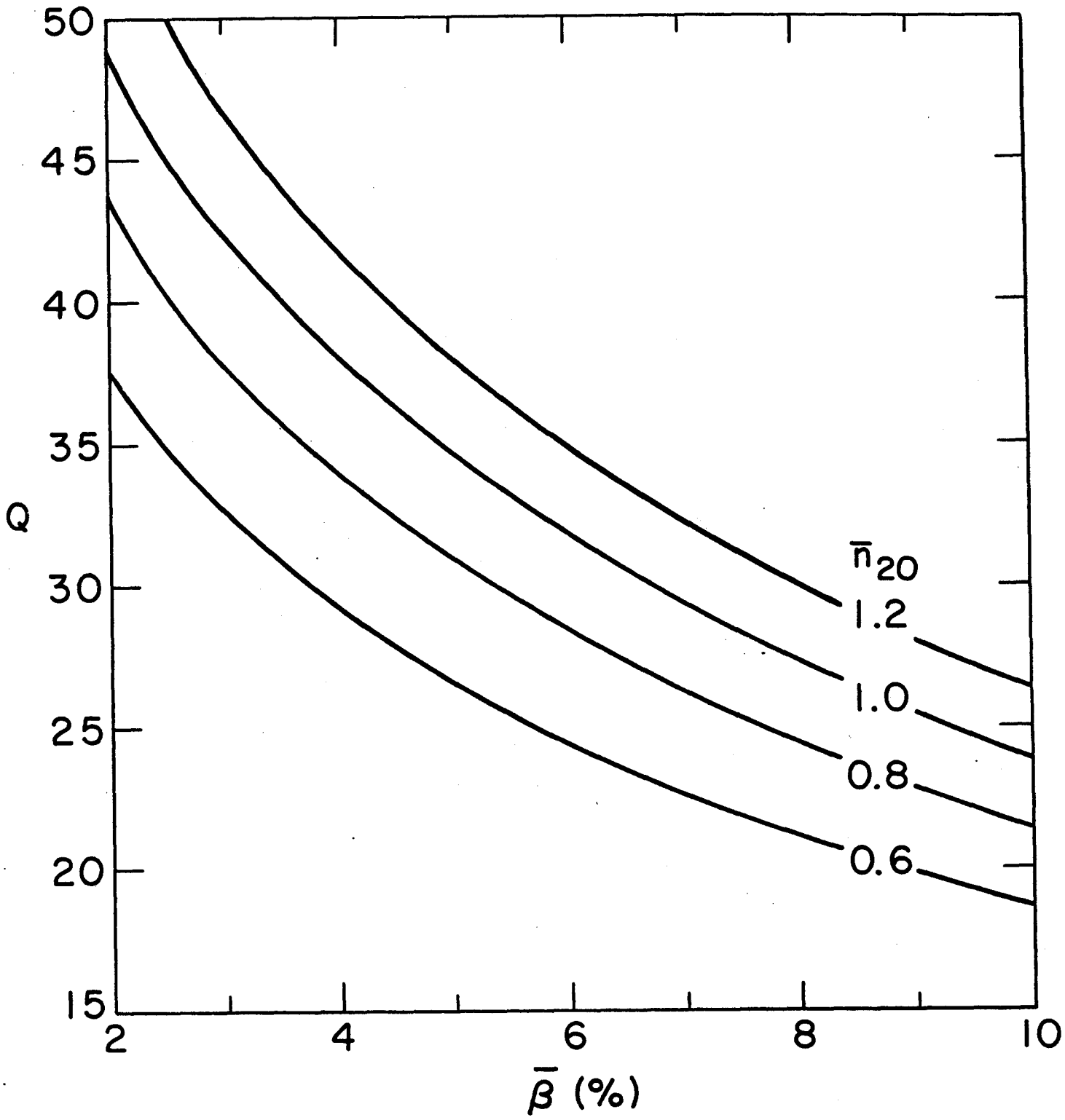

FIG. 15. Fusion to rf power ratio versus averaged toroidal beta for several plasma densities. [R = 6 m, A=5, S = 1, $\bar{T}_e$ = 15 KeV, $\bar{T}_i$ = 22 KeV, $n_e = n_{eo}(1 - \rho^3)$, $T = T_o(1 - \rho^2)$, $J = J_o(1 - \rho^2)$, $\omega = 2\omega_{LH}(0)$].

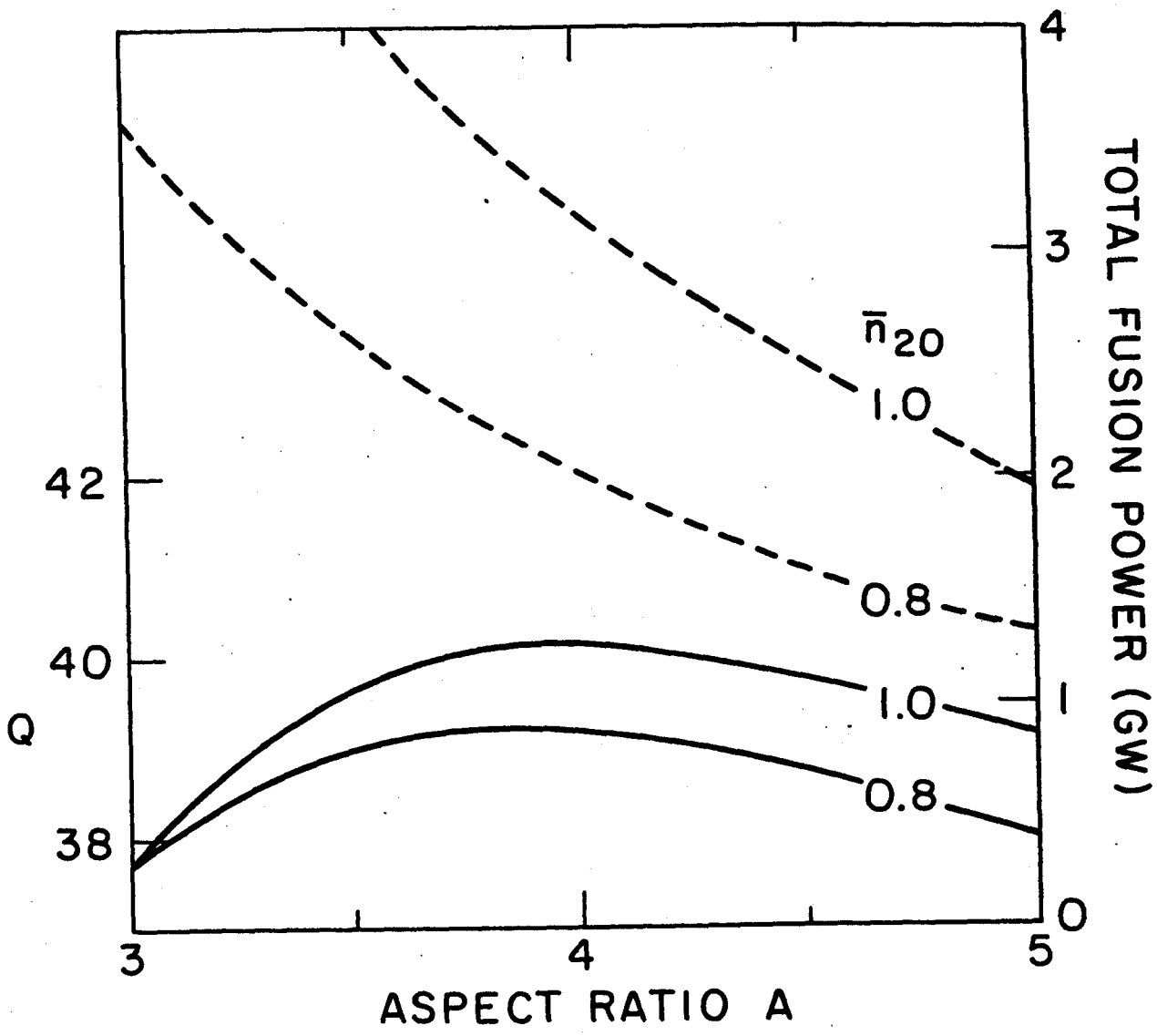

FIG. 16. Fusion to rf power ratio (solid curves) and the corresponding total fusion power (dashed curves) versus aspect ratio for two plasma densities. [R = 6 m, B_{To} = 13 T, d = 1.4 m, S = 1.5, $\bar{T}_e$ = 15 KeV, $\bar{T}_i$ = 22 KeV, $n_e = n_{eo}(1 - \rho^3)$, $T = T_o(1 - \rho^2)$, $J = J_o(1 - \rho^2)$, f = 2.48 - 2.75 Ghz].

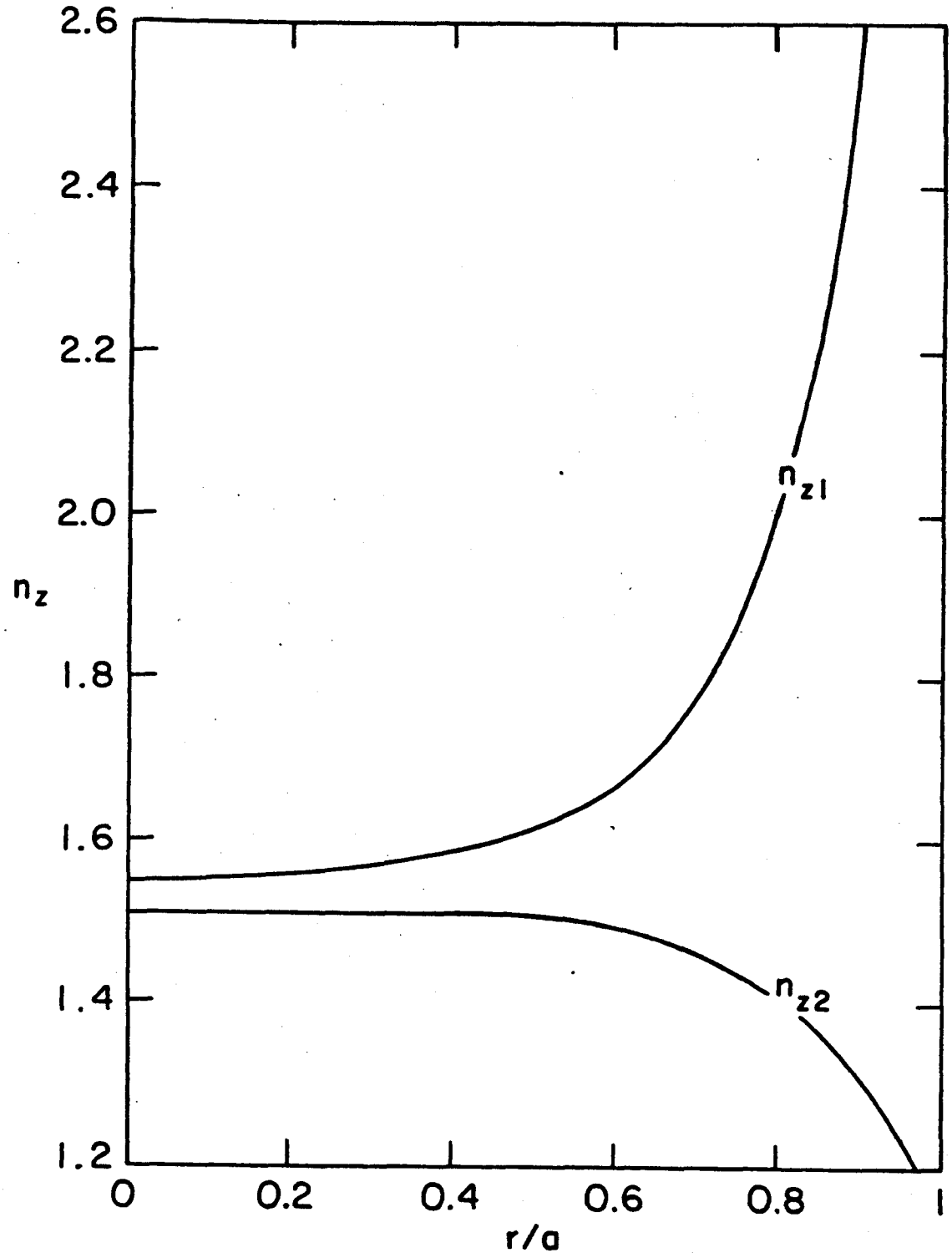

FIG. 17. Spectrum of lower hybrid wave as a function of radial position necessary to provide the Q for the reference reactor of Table 1.

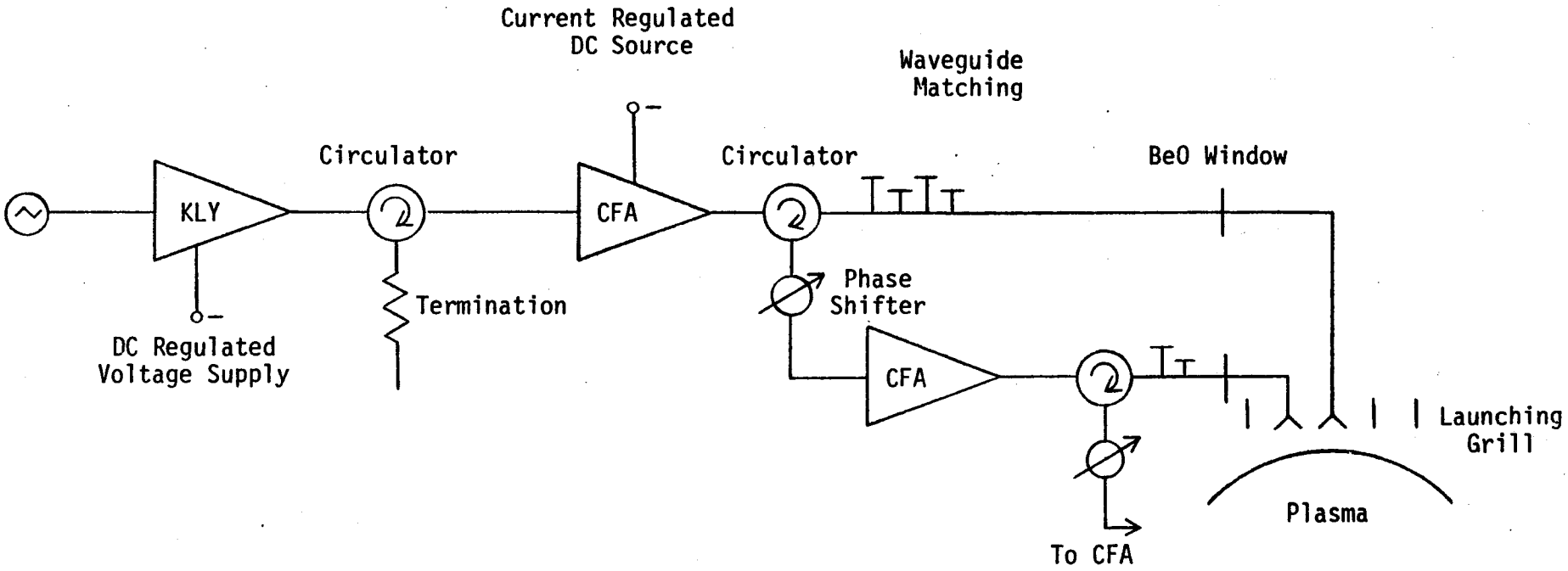

Fig. 18 High Efficiency RF Auxiliary Heating and Toroidal Current Driving System with Direct Energy Recovery

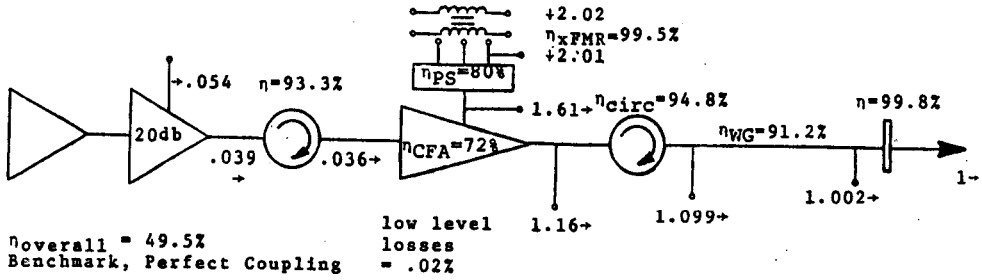

$\eta_{overall}$ = 49.5%
Benchmark, Perfect Coupling

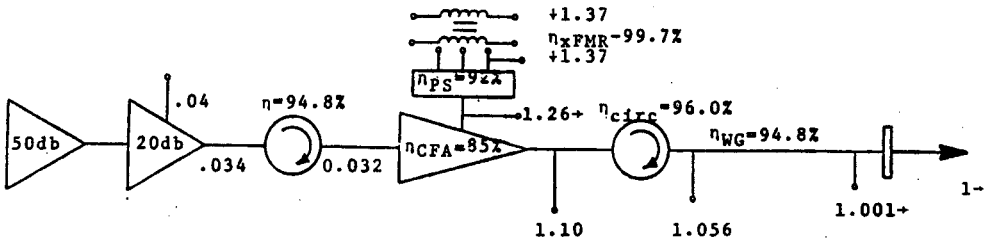

$\eta_{overall}$ = 73.0%
Developmental, Perfect Coupling

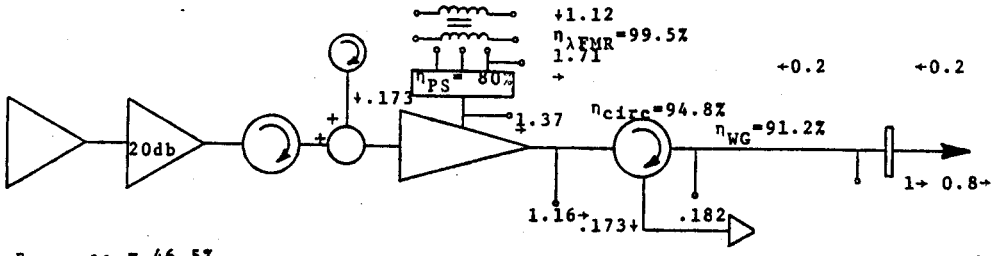

$\eta_{overall}$ = 46.5%
Benchmark, 80% Efficient Coupling
with Direct Energy Recovery

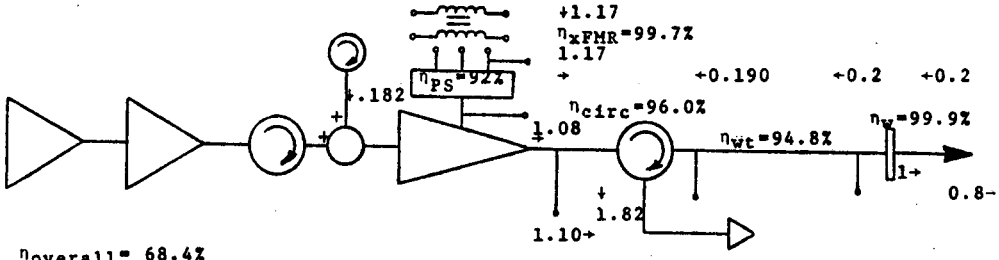

$\eta_{overall}$= 68.4%
Developmental, 80% Efficient Coupling
with Direct Energy Recovery

Figure 19

Loss Inventories for Microwave Power Delivery Systems for Perfect and 80% Coupling to the Plasma